Quaternary Science Reviews 28 (2009) 1631–1657

Contents lists available at ScienceDirect

Quaternary Science Reviews

journal homepage: www.elsevier.com/locate/quascirev

Calibrating a glaciological model of the Greenland ice sheet from the Last Glacial Maximum to present-day using field observations of relative sea level and ice extent

Matthew J.R. Simpson [a,*], Glenn A. Milne [a,1], Philippe Huybrechts [b], Antony J. Long [c]

[a] Department of Earth Sciences, Durham University, Science Site, South Road, Durham DH1 3LE, UK
[b] Earth System Sciences and Departement Geografie, Vrije Universiteit Brussel, B-1050 Brussels, Belgium
[c] Department of Geography, Durham University, Science Site, South Road, Durham DH1 3LE, UK

ARTICLE INFO

Article history:
Received 29 September 2008
Received in revised form
9 March 2009
Accepted 11 March 2009

ABSTRACT

We constrain a three-dimensional thermomechanical model of Greenland ice sheet (GrIS) evolution from the Last Glacial Maximum (LGM, 21 ka BP) to the present-day using, primarily, observations of relative sea level (RSL) as well as field data on past ice extent. Our new model (Huy2) fits a majority of the observations and is characterised by a number of key features: (i) the ice sheet had an excess volume (relative to present) of 4.1 m ice-equivalent sea level at the LGM, which increased to reach a maximum value of 4.6 m at 16.5 ka BP; (ii) retreat from the continental shelf was not continuous around the entire margin, as there was a Younger Dryas readvance in some areas. The final episode of marine retreat was rapid and relatively late (c. 12 ka BP), leaving the ice sheet land based by 10 ka BP; (iii) in response to the Holocene Thermal Maximum (HTM) the ice margin retreated behind its present-day position by up to 80 km in the southwest, 20 km in the south and 80 km in a small area of the northeast. As a result of this retreat the modelled ice sheet reaches a minimum extent between 5 and 4 ka BP, which corresponds to a deficit volume (relative to present) of 0.17 m ice-equivalent sea level. Our results suggest that remaining discrepancies between the model and the observations are likely associated with non-Greenland ice load, differences between modelled and observed present-day ice elevation around the margin, lateral variations in Earth structure and/or the pattern of ice margin retreat.

1. Introduction

Since the Last Glacial Maximum (LGM, 21 ka BP), the Earth has seen the decay of the great ice sheets covering North America and Eurasia, ice mass loss in Greenland and Antarctica and the reduction of mountain glaciers. Over this time, global mean sea level has risen c. 120 m (e.g. Fairbanks, 1989; Yokoyama et al., 2000). This large ice–ocean mass exchange together with rapid climate change in Greenland (e.g. Cuffey et al., 1995) has played a part in the evolution of the Greenland ice sheet (GrIS) over this period. At the LGM, the GrIS is thought to have extended to cover parts of the continental shelf (Funder and Hansen, 1996) and reached an excess volume (compared to present) of 2–3 m ice-equivalent sea level (Clark and Mix, 2002). The retreat of the GrIS is hypothesised to have occurred in two key stages (Funder, 1989); initial retreat was driven by sea-level rise, causing the calving of ice grounded below sea-level and break up of the marine portions of the ice sheet. By c. 10 ka BP the GrIS was essentially at or inland of the present-day coastline (Funder and Hansen, 1996; Bennike and Björck, 2002). The second phase of retreat during the Holocene (10 ka BP to present) was slower and driven, primarily, by surface melting. Of particular interest is the reaction of the GrIS to the peak warming period known as the Holocene Thermal Maximum (HTM). The response of the ice sheet to this forcing may be a useful analogue for its future behaviour in a warming climate. The HTM occurred, broadly, between 9 and 5 ka BP in Greenland (Kaufman et al., 2004) causing the ice sheet to retreat behind its present-day position and reach a minimum post-LGM volume. It is not clear where and how far the ice margin retreated inland of its current position, as subsequent to reaching this minima the GrIS experienced a neoglacial readvance (Kelly, 1980), and so all geological and geomorphological evidence of the minimum configuration was overridden by advancing ice.

* Corresponding author. Tel.: +44 0191 3342300.
E-mail address: m.j.r.simpson@dur.ac.uk (M.J.R. Simpson).
[1] Present address: Department of Earth Sciences, University of Ottawa, Ontario, K1N 6N5, Canada.

0277-3791/$ – see front matter
doi:10.1016/j.quascirev.2009.03.004

Today the GrIS holds enough ice volume to raise mean global sea level by c. 7 m (Bamber et al., 2001). Recent mass balance estimates based on geodetic observations generally indicate an accelerated mass loss from Greenland over the last decade (Lemke et al., 2007). Due to the short time span of these observations, however, it remains contested if these changes are the beginning of a sustained response of the ice sheet to recent warming. The interpretation of these data is further complicated by the ongoing vertical motion of the solid Earth to past ice sheet changes. This contaminant signal is predicted using models of glacial isostatic adjustment (GIA) and removed from the measured signal. It is clear that a good understanding of past GrIS evolution is required if present-day observations are to be interpreted correctly.

The overall aim of this work is to calibrate a glaciological model of GrIS evolution since the LGM using inferences of relative sea level (RSL) and past ice extent from field data. The analysis has three primary motivations: (i) such a model can provide important insight into how the GrIS reacted to past sea-level and climate change and thus inform us how the ice sheet might behave in the future; (ii) as stated above, such a model can be adopted to predict the pattern of present-day solid Earth deformation in Greenland to more accurately correct and interpret the growing quantity and variety of geodetic data; and (iii) calibrating a model to field data will highlight any particular weaknesses in the ice and Earth model adopted and can therefore guide future research into model development.

Three approaches can be employed to reconstruct the deglaciation history of ice sheets: (1) three-dimensional ice sheet models that are forced by prescribed climatic conditions and freely simulate past ice sheet evolution (e.g. Huybrechts, 1990); (2) observations of GIA-induced sea-level change in the near-field of past or presently glaciated regions that are used to quantitatively infer the loading history of grounded ice sheets (e.g. Peltier, 1994); and (3) directly constraining the lateral and/or height extent of past ice from field observations (e.g. Dyke and Prest, 1987; Bentley et al., 2006). Previous studies have, in general, combined only two of these approaches; normally (1) and (3) (e.g. Marshall et al., 2002) or (2) and (3) (e.g. Tushingham and Peltier, 1991). The Greenland GrB model of Tarasov and Peltier (2002) first demonstrated that by adopting (1) a 3-D ice sheet model with (2) a GIA forward model is a powerful tool that reduces the uncertainty of past ice sheet evolution. In this study we combine and apply all three methods (e.g. Tarasov and Peltier, 2004) to the Greenland ice sheet. Using, primarily, observations of RSL complemented by geological and geomorphological data we constrain the millennial-scale spatial changes of a 3-D thermomechanical ice sheet model (Huybrechts, 2002) from the LGM to the present-day.

Two previous studies have constrained the evolution (LGM to present-day) of the GrIS using RSL data. First, as mentioned above, Tarasov and Peltier (2002) presented their GrB model which forms the Greenland component of the global ice sheet reconstruction ICE-5G (Peltier, 2004). Second, Fleming and Lambeck (2004) presented their GREEN1 model which has a deglaciation history based on several stages of linear interpolation between an LGM reconstruction (Denton and Hughes, 1981) and the observed present-day ice sheet (Ekholm, 1996). We extend these previous studies in two main respects: (i) we make use of an RSL and ice extent dataset that is significantly improved over those used in these past two analyses. In particular, previous models were constrained primarily using sea-level observations derived from molluscan assemblages which have a large age and altitude uncertainty. We focus on the growing number of RSL observations reconstructed from isolation basins (e.g. Long et al., 2006, 2008, in press; Sparrenbom et al., 2006a, b) which are more precise and consequently provide a more powerful model constraint (see Section 2.1); (ii) we provide a more detailed sensitivity analysis which targets key Earth and ice model parameters.

The work is structured as follows; in Section 2.1 we describe the nature of the data employed to calibrate the ice model and provide an overview of the observed sea-level history of Greenland. We start our modelling (Section 3) by comparing predictions generated using the ice model published by Huybrechts (2002). Adopting this as our preliminary ice model, we consider the sensitivity of sea-level predictions to wide ranges in the more important Earth model parameters and identify an optimal set of values. Based on this Earth model sensitivity study, we are able to isolate data-model misfits that are due to limitations in the ice model. We then explore key aspects of the ice history that might explain the misfits of our starting ice model (Section 3.2). A central element of our analysis is the careful examination of trade-offs between ice and Earth model parameters. In Section 3.3 we show fits to the RSL data for our new calibrated ice model, before discussing the key aspects of our new model (Section 4.1) and possible sources for any remaining data-model residuals (Section 4.2). The conclusions are listed in Section 5.

2. Data and description of the model

2.1. Nature of the data

In our modelling analysis we use data on past RSL and past ice extent. The primary focus is upon RSL data, the locations and source references of which are shown in Fig. 1 and Table 1, respectively. All RSL data used in this investigation are categorised as either sea-level index points or limiting dates. In total there are 214 observations used for RSL reconstruction; 73 of which have a well defined height and age relationship to former sea level and a further 141 that provide limiting constraints. Sea-level index points are derived from field evidence that has a defined (c. $\pm$50 cm) vertical relationship to past mean sea level. This height relationship is referred to as the 'indicative meaning' (e.g. Shennan, 1986). In Greenland, the most precise sea-level index points are derived from dating the sediments preserved in isolation basins (e.g. Bennike, 1995; Long et al., 1999; Sparrenbom et al., 2006a) and thus provide a precise measure of past sea level in both time and height. By analysing a staircase of basins that occur below the marine limit, a well constrained RSL reconstruction can be produced (e.g. Fig. 2).

A variety of other field evidence lack an indicative meaning (a defined height relationship to a former tidal datum) and so provide a less precise height constraint on past sea level; these are referred to as limiting dates. Radiocarbon dates from marine shells within raised beaches or deltas are typical examples of limiting dates. It is often uncertain how far below past sea level the shells lived and in most instances they provide only a lower height limit for RSL reconstructions (Gotfredsen and Møberg (2004) detail the height relationship to mean sea level for specific molluscan species). However, for a number of shell dates plotted on a time–height diagram the upper height envelope of these observations can often tentatively be interpreted as past mean sea level. Fig. 2 shows a comparison of limiting dates (Rasch and Jensen, 1997) with index point data from an isolation basin study from Innaarsuit (Inn, Fig. 1) in southern Disko Bugt. We select limiting dates that are close to the isolation basins to keep spatial differences in RSL small. Using only the isolation basin data as a guide we reconstruct past sea level on the time–height diagram (dashed line, Fig. 2) and on top of which the limiting dates are also plotted. Mostly we find the upper height envelope of the shell dates corresponds (within age error) to the past sea-level reconstruction. With more and better time–height coverage of the data we can have increasing confidence that the

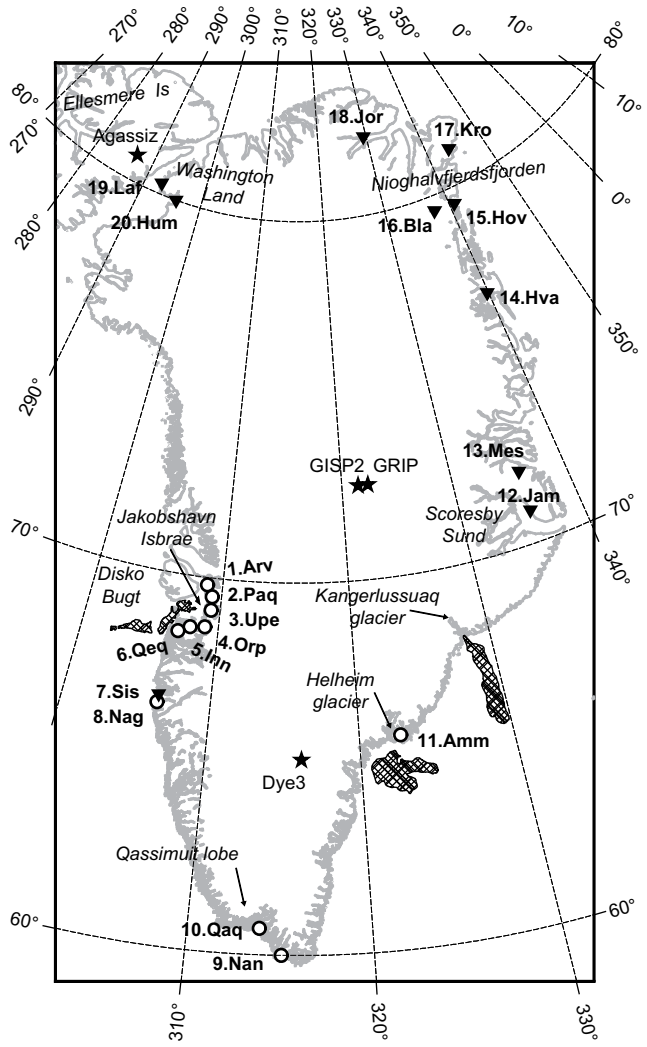

Fig. 1. Map showing the locations of the RSL observations used in this study as well as place names referred to in the text. Circles and inverted triangles mark, respectively, the locations of index point data and limiting data used in this analysis. Stars mark locations of ice core sites mentioned in the text. The crosshatched areas mark cross-shelf troughs associated with the named outlet glaciers. Table 1 lists RSL observations used and source literature.

upper height envelope of the shell dates can be interpreted as past sea level.

All of the limiting dates presented in the following analyses are assigned a height error that relates to the elevation sampling error and, importantly, not to their indicative meaning. Unless otherwise stated in the source literature we follow previous authors by ascribing a sampling elevation height error of ±5 m for marine shells and ±2 m for archaeological or freshwater organic material (Rasch and Jensen, 1997). Given the uncertainties inherent in the limiting dates we quantify data-model fits in two ways; (i) that limiting dates only provide a height limit and (ii) on the assumption the upper height envelope of the shell dates lies close to past mean sea level. For most of the analyses we consider limiting dates as only a height limit. In this case an RSL prediction would give fit to a shell date if it plotted either within the elevation error or above the date. For the analysis in Sub-Section 4.2.3 we assume that, for a given locality, the upper height envelope of the shell dates lies close to past mean sea level and a fit is achieved only if the prediction plots within the elevation error of these specific dates.

All radiocarbon dates used in this study have been calibrated using the programme CALIB Rev5.0.1 (Stuiver and Reimer, 1993) with the Intcal04 curve (Reimer et al., 2004) and are cited with a two-sigma age range. All dates given are in calibrated years. As adopted by Bennike and Björck (2002) a reservoir correction of 400 years is applied to marine samples from the west coast and a correction of 550 years to samples from the north and east coasts.

An additional RSL constraint that we use is the height of the Holocene Marine Limit (HML). The HML is traditionally thought to have formed immediately after deglaciation and is often marked by the lowest limit presence of perched boulders. The HML represents the highest point of past sea level for an ice-free region. In Greenland traceable contours of the HML define uplift domes that run parallel to the coast and characterise the emergence of the solid Earth from the sea surface (Funder and Hansen, 1996; Weidick and Bennike, 2007). It is possible to date the HML but organic material is often sparse and so, in many localities, it is necessary to extrapolate dates of material found at lower altitudes. Alternatively, lakes above the HML can be dated to determine the onset of organic accumulation and thus establish when an area became ice-free (Long et al., 2008).

As indicated above, we also consider field evidence pertaining to the past lateral extent of the GrIS. Geological and geomorphological features show how the ice sheet retreated from its maximum extent on the continental shelf (e.g. Evans et al., 2002) and radiocarbon dates can provide the minimum age of deglaciation for presently ice-free areas (e.g. Bennike and Björck, 2002).

2.2. Description of the glacial isostatic adjustment model

The GIA forward model is comprised of a sea-level model, an ice sheet model and a model of Earth rheology. The first two model components define the ice–ocean mass exchange which represents the forcing, whilst the isostatic response is governed by the prescribed Earth structure and rheology.

We adopt the three-dimensional thermomechanical ice sheet model of Huybrechts (2002) as a starting Greenland ice load (hereafter referred to as 'Huy1'). The Huy1 model simulates the evolution of the Greenland ice sheet over the last two glacial cycles in response to changes in past climate and eustatic sea level. The model is comprised of three parts; calculating ice-dynamics, solid Earth (isostatic) response and mass balance (see Huybrechts and de Wolde (1999) for a full description). There are 31 layers in the vertical and a horizontal grid resolution of 20 km, which corresponds to 83×141 horizontal grid cells for Greenland. Ice-dynamics are simplified to the shallow ice approximation for large ice masses (Hutter, 1983). Grounded ice flows through internal deformation and basal sliding. Longitudinal stress is ignored and grounding-line dynamics are not modelled. The Earth model of Huy1 should not be confused with the one employed in this study; Huy1 has an asthenosphere with a single relaxation time (3000 years) overlain by an elastic lithosphere. Overall mass balance is considered as the net contribution of the input (snowfall accumulation) and outputs (meltwater runoff and calved ice) to the ice sheet system. Meltwater runoff is calculated using the positive degree day method (e.g. Braithwaite, 1995) which takes the melt rate to be proportional to the surface air temperature. Huy1 uses the recalibrated runoff model of Janssens and Huybrechts (2000). The sea-level and climate forcing are outlined in Sub-Sections 3.2.2 and 3.2.3, respectively. The non-Greenland component of the ice load is represented by the global ice sheet model ICE-5G (Peltier, 2004).

Farrell and Clark (1976) presented the seminal work on sea-level change as a result of Earth glaciation. Their theory is encompassed by the 'sea-level equation', which has undergone a number of developments over the last 30 years that have improved the method of solution and/or extended the theoretical basis

Table 1
RSL observations used in this study to constrain our GIA model.

Region	Site	Site name	Source Publication
West	1	Arveprinsen (Arv)	(Long et al., 1999)
	2	Paqitsoq (Paq)	(Long et al., 2006)
	3	Upernivik (Upe)	(Long et al., 2006)
	4	Orpissooq (Orp)	(Long and Roberts, 2002)
	5	Innaarsuit (Inn)	(Long et al., 2003)
	6	Qeqertarsuatsiaq (Qeq)	(Long and Roberts, 2003)
Southwest	7	Sisimiut (Sis)	(Kelly, 1979; Weidick, 1972)
	8	Natoralinguaq (Nag)	(Long et al., in press)
South	9	Qaqortoq (Qaq)	(Sparrenbom et al., 2006b)
	10	Nanortalik (Nan)	(Bennike et al., 2002; Sparrenbom et al., 2006a)
Southeast	11	Ammassalik (Amm)	(Long et al., 2008)
East	12	Jameson Land (Jam)	(Funder and Hansen, 1996)
	13	Mesters Vig (Mes)	(Trautman and Willis, 1963; Washburn and Stuiver, 1962)
Northeast	14	Hvalrosodden (Hva)	(Landvik, 1994)
	15	South Hovgaard Ø and northeastern Lambert Land (Hov)	(Bennike and Weidick, 2001)
	16	Blåsø (Bla)	(Bennike and Weidick, 2001)
	17	Kronprins Eijland (Kro)	(Hjort, 1997)
North	18	Jorgen Brunlund Fjord (Jor)	(Funder and Abrahamsen, 1988)
Northwest	19	Lafayette Bugt (Laf)	(Bennike, 2002)
	20	Humboldt Gletscher (Hum)	(Bennike, 2002)

The locations are marked in Fig. 1.

(e.g. Nakada and Lambeck, 1987; Mitrovica and Peltier, 1991; Johnston, 1993; Milne and Mitrovica, 1996; Milne et al., 1999; Mitrovica and Milne, 2003). We do not go into theoretical detail in this study; the most recent advances and a review of the sea-level equation (as applied in this analysis) are described by Mitrovica and Milne (2003) and Kendall et al. (2005). In general terms, the sea-level model predicts the vertical deflection of both the ocean surface and the Earth's solid surface due to changes in ice–ocean mass configuration. Height shifts of the ocean surface are determined by computing perturbations to the geopotential. Changes to this field can be split into: (i) the direct effect – the gravitational effect caused by changes in ice–ocean mass configuration and associated changes to rotational potential and (ii) the indirect effect – the gravitational effect caused by internal mass flux of the solid Earth and associated changes to rotational potential. Global ice/water mass is conserved in the model.

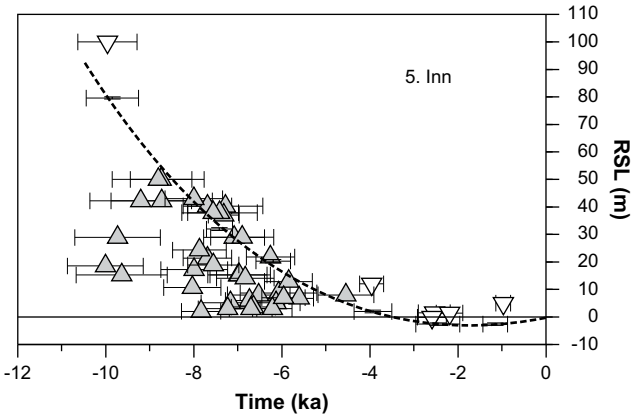

Fig. 2. A comparison of isolation basin data (index points) and marine shell and archaeological data (lower and upper limiting dates) from southern Disko Bugt. Lower limiting dates are shown as grey triangles. Upper limiting dates are shown as inverted white triangles. Sea-level index points are represented by both time and height error bars. The black dashed line represents the sea-level reconstruction based on the isolation basin data. An overall fall in RSL indicates that the solid Earth has rebounded and thus the ice sheet has undergone a local mass loss.

Following Peltier (1974), the GIA ice–ocean forcings are convolved with the impulse response Love numbers for a spherically symmetric, visco-elastic, self-gravitating and compressible Earth model. The elastic and density structure are taken from seismic constraints (Dziewonski and Anderson, 1981) and depth parameterised with a resolution of 15–25 km. The radial viscosity structure is depth parameterised to give an elastic lithosphere (i.e. very high viscosity values are assigned), an isoviscous upper mantle bounded by the base of the lithosphere and the 670 km deep seismic discontinuity, and an isoviscous lower mantle continuing below this depth to the core-mantle boundary. For convenience we define a reference Earth model with a lithospheric thickness of 96 km and upper and lower mantle viscosities of 5×10^{20} Pa s and 10^{22} Pa s, respectively. These parameters fall near the middle of the range of values inferred in recent GIA modelling studies (e.g. Mitrovica and Peltier, 1993, 1995; Peltier, 1996; Peltier and Jiang, 1996; Mitrovica and Forte, 1997, 2004; Lambeck et al., 1998; Kaufmann and Lambeck, 2000, 2002) and so our reference model can be considered as a useful intermediate model for comparison purposes.

3. Modelling results

3.1. Sea-level predictions based on the Huy1 model

Here we present sea-level predictions generated from our GIA model using the ice history Huy1. The aims of this section are to: (i) examine sensitivity of the predictions to changes in Earth viscosity structure; (ii) determine a best-fit Earth model to partner Huy1 and (iii) assess whether acceptable data-model fits can be obtained using the Huy1 ice model and a spherically symmetric Earth model.

3.1.1. Sensitivity of predictions to Earth viscosity structure

Making changes to Earth parameters alters the isostatic response to a given surface load. We start by focussing on one site – Arveprinsen in west Greenland (Arv, Fig. 1) – to provide a general example and explain how the envelopes of predictions shown in subsequent analyses are generated.

Fig. 3 shows RSL predictions at Arveprinsen for our reference model (dashed-dotted black line) and six other models which are the same as the reference model except for one parameter value. The solid lines show predictions for a model Earth in which the lithospheric thickness has been increased to 120 km (grey) or decreased to 71 km (black). Comparing these curves shows that this range of lithospheric thickness has a significant influence on the magnitude of the RSL prediction but little impact on the shape of the curve. In contrast, changing the value of viscosity in the upper or lower mantle affects both the magnitude and the shape of the curve. The dashed lines show the sensitivity of the predictions to changing the viscosity in the upper mantle from a value of 3×10^{20} Pa s (black) to 10^{21} Pa s (grey). The dotted lines show the influence of varying lower mantle viscosity from 10^{21} Pa s (black) to 5×10^{22} Pa s (grey). In general, lower viscosity values permit a more rapid isostatic response to a given loading event (e.g. note the more rapid sea-level fall of the black dashed line compared to the grey dashed line following local ice unloading at ~15 ka BP). One important point to note from this sensitivity study is that the timing of the initial RSL fall is not affected by these Earth model changes and so is controlled by changes in ice load.

We generated predictions at Arveprinsen for a suite of 108 different Earth viscosity models that sample the range of values specified above. The grey shaded region in Fig. 3 bounds the suite of predictions generated from these model runs and so illustrates the sensitivity of the predictions at this site to a large range of plausible Earth viscosity models. Note that the bounds of these envelopes may well be defined by more than one prediction. The envelopes can be considered as a measure of the uncertainty in the predictions associated with limited knowledge of mantle viscosity structure. We show these envelopes for all the data sites in Section 3.1.3 to examine whether the Huy1 model is consistent with the data to within this uncertainty.

3.1.2. Determining an optimal viscosity model

We compute RSL at all 20 data sites considered for each of the 108 Earth models introduced above and quantify the goodness of fit for each Earth model using the χ^2 criterion:

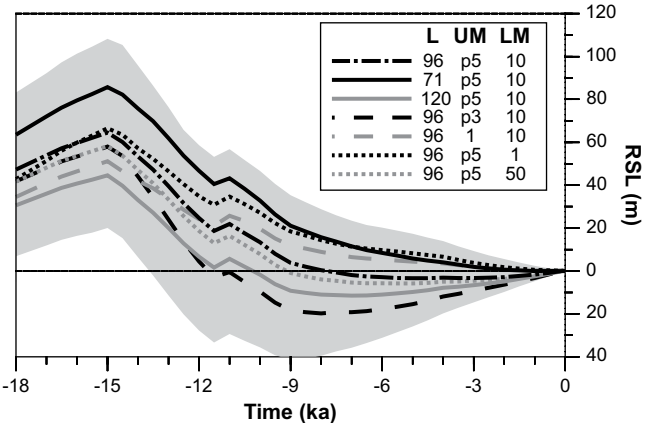

Fig. 3. Sensitivity of sea-level predictions at Arveprinsen to changes in Earth viscosity structure. All changes are relative to our reference Earth structure which has a 96 km thick lithosphere, upper mantle viscosity of 0.5×10^{21} Pa s and lower mantle viscosity of 10^{22} Pa s. Predictions for this model are shown by the dashed-dotted black line. Shown are predictions for lithospheric thicknesses of 71 km (solid black) and 120 km (solid grey), upper mantle viscosities of 0.3×10^{21} Pa s (dashed black) and 10^{21} Pa s (dashed grey) and lower mantle viscosities of 10^{21} Pa s (dotted black) and 50×10^{21} Pa s (dotted grey). The grey shaded region denotes the variation in RSL for 108 model runs that sample the viscosity parameter ranges defined above.

$$\chi^2 = \frac{1}{n}\sum_{i=1}^{n}\left(\frac{y_i^{\mathrm{pr}} - y_i^{\mathrm{obs}}}{\sigma_i}\right)^2. \quad (1)$$

The χ^2 value indicates the difference between predicted (y_i^{pr}) and observed sea level (y_i^{obs}) for a specified observational error (σ_i) and given RSL data point (i). A value of one or less indicates a fit to the data (within error) whilst a misfit can produce a very large value due to the squared term. In this first analysis limiting dates are considered only as height limits and therefore can still give fit even when there are large differences between the model results and the elevation height error. If predicted sea level passes above a shell date, for example, then a fit is still achieved due to the associated uncertainty of lower limiting data and its relationship to contemporaneous sea level. In this situation the χ^2 value is assigned a value of one. Fig. 4 shows how the goodness of fit varies with upper and lower mantle viscosity for lithospheric thicknesses of 71, 96 and 120 km. We see a general pattern of increasing data-model misfit for smaller upper mantle and larger lower mantle viscosities. The misfit also increases as the lithosphere is thickened. The 71 km pane shows a zone of relatively good fit for middling values of upper and lower mantle viscosities; this area represents the best-fit Earth model for Huy1. Specifically, a model characterised by a 71 km lithosphere, an upper mantle viscosity of 5×10^{20} Pa s and a lower mantle viscosity of 5×10^{21} Pa s provides the optimum fit. It is worth noting that the χ^2 test and best-fit model will have a bias toward fitting the west Greenland dataset as: (1) there are numerous data from this region and (2) the data here are mostly from isolation basins which have good height precision and so the χ^2 values will increase quickly with an increasing misfit.

3.1.3. Comparison of Huy1 model to RSL observations

In the near-field of Greenland we can expect that a primary control on past sea-level change is the isostatic adjustment of the solid Earth due to changes in the load distribution of the GrIS. This is reflected in the field observations which, at most localities, show an overall fall in RSL from Lateglacial time to the present-day (Fig. 5), indicating that the solid Earth has rebounded and thus the ice sheet has undergone a mass loss. Clearly, patterns of past sea-level change vary across Greenland – a more detailed discussion of regional sea-level variation follows in this subsection. These inter-regional differences in RSL change can be used to infer the pattern of ice sheet evolution at various levels of sophistication: from the direct interpretation of maps of the HML to identify regions that have experienced greatest ice load loss (Funder and Hansen, 1996; Weidick and Bennike, 2007) to the more involved geophysical modelling studies that constrain 3-D models of GrIS history (Tarasov and Peltier, 2002; Fleming and Lambeck, 2004).

Isolation basin studies (e.g. Long et al., 1999; Bennike et al., 2002; Sparrenbom et al., 2006a) have shown that in some areas Holocene RSL fall continued to a height below present-day sea level (e.g. Fig. 5a, site 1). When RSL does fall below present-day sea level it is followed by a small rise which gives the curve a characteristic 'J-shape'. This shows that sea level in some areas of Greenland underwent a late Holocene transgression; a change also evident from archaeological studies of paleo-Eskimo sites which are now partly submerged (e.g. Hjort, 1997; Rasch and Jensen, 1997; Mikkelsen et al., 2008). Eustatic sea-level change is thought to have decelerated during the mid-Holocene from a rate of c. 1 to 0 m/ka by 2 ka BP (e.g. Lambeck and Purcell, 2005) and so the RSL switch likely represents a change from rebound to subsidence of the solid Earth surface. Past sea-level investigations have attributed the RSL switch to a downward deflection of the solid Earth as the result of both/either (i) the collapse of a forebulge and/or (ii) the

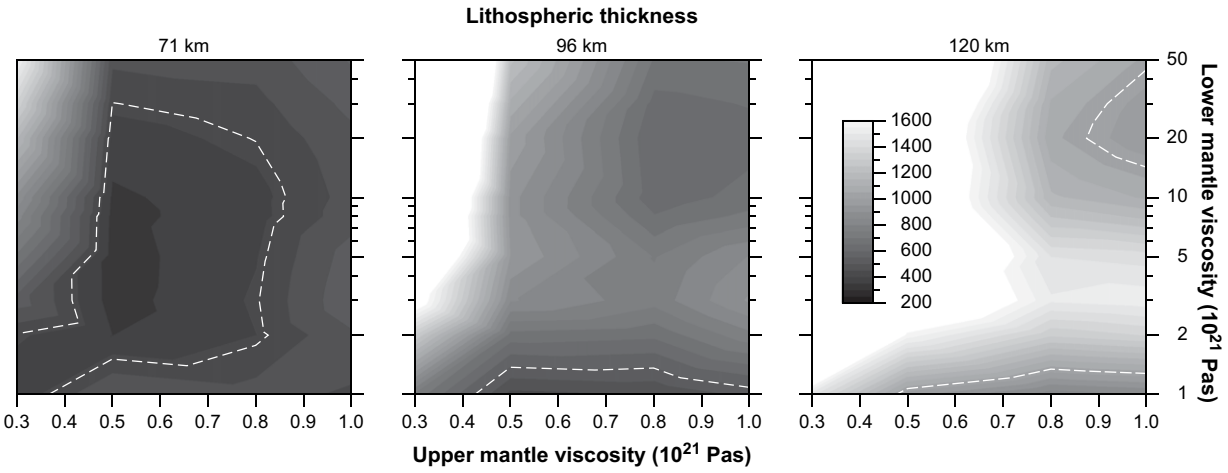

Fig. 4. The Chi-squared results for the Huy1 ice model and 108 different Earth viscosity models (see text for details). Each frame is based on a fixed value for lithospheric thickness (as indicated). The scale bar for the Chi-squared results is shown in the right-hand frame. The 95% confidence level is marked by the white dashed line.

neoglacial ice loading in Greenland (Kelly, 1980; Weidick, 1993; Long et al., 1999).

Beginning in west Greenland and working anti-clockwise we briefly review the RSL history of each region and compare predictions to the observations (Fig. 5). In grouping the data into single RSL curves we used the model to check that spatial differences in RSL predictions were small. In general, for a given site, the data are clustered within an area of dimension less than a few 100s km^2.

Situated on the central west Greenland coast, the marine embayment of Disko Bugt has become a classic area for sea-level investigations. Studies on Disko Island (Ingolfsson et al., 1990) and in Disko Bugt (Rasch, 2000) show a clear decline of the HML from c. 120 m in southeast Disko Bugt to c. 60 m in northwest Disko. It is well established that Disko Bugt sits upon the northern flank of a high uplift dome that runs parallel to much of the ice-free southwest coast (first mapped by Weidick (1976)). Numerous RSL isolation basin investigations (Long et al., 1999, 2003, 2006) have shown conclusively that after a rapid early Holocene fall, RSL fell below present-day sea level c. 5–4 ka BP to reach a lowstand c. 2 ka BP before rising 1–5 m to present. Comparing the predictions to the data in this area (sites 1–6, Fig. 5a) indicates that the fall from the HML occurs too early and at too low a rate. In addition, at all of these sites the best-fit sea-level prediction fails to provide fit to the oldest index point.

In southwest Greenland (sites 7 and 8, Fig. 5a) best-fit predicted sea level reaches a height of c. 100 m, this is around 20 m below the HML (Funder and Hansen, 1996). It should be noted that for Sisimiut (site 7) we have omitted the partially published dates of Petersen and a dated whale cranium which is presumed to be contaminated (Kelly, 1979). The lower limiting dates from Sisimiut suggest a rapid fall in RSL from c. 100 m at 10 ka BP to close to present-day sea level by 6 ka BP. Further south at Nagtoralinguaq (site 8) new sea-level index points have revealed that RSL dipped c. 4 m below present-day sea level at around 2 ka BP (Long et al., in press). For southwest Greenland, modelled RSL fall is too early and too slow, while the magnitude of the signal is under predicted (in contrast to sites in the central west).

A map of the HML in south Greenland (Fig. 5 in Weidick et al., 2004) shows a drop from c. 60 m near the Qassimiut lobe to c. 20 m at the southern tip of Greenland. At Qaqortoq and Nanortalik (sites 9 and 10, Fig. 5b), RSL falls below present-day sea level at c. 10–9 ka BP, earlier than recorded anywhere else in Greenland. At Qaqortoq the prediction shows some agreement with the index point data but does not reach the HML. Other evidence from a drowned isolation basin at this site indicates that RSL fell 6–8 m below present-day sea level (Sparrenbom et al., 2006b) – this is not captured in the model predictions. RSL at Nanortalik is predicted to be largely negative and the best-fit prediction is 30–40 m below the HML. The two earliest index points from Nanortalik come from a lake situated offshore which is c. 15 km from the cluster of other lakes cored and so including these on the same RSL plot is not strictly appropriate (Sparrenbom et al., 2006a).

Ammassalik (site 11, Fig. 5b) represents the only RSL data from the southeast of Greenland. Two cored lakes show that ice-free conditions were established here c. 11 ka BP, which is also interpreted to be the time RSL fell from the HML (c. 70 m) (Long et al., 2008). There is a c. 50 m misfit between the HML and best-fit predicted sea level at this time. The lowest lying lake is at c. 1 m and shows no marine incursion from 6.7 ka BP to present-day. During this period RSL must have been below the height of the lake. These results indicate that Huy1 significantly underestimates the magnitude of ice unloading in this area.

In east Greenland, RSL predictions for Jameson Land (site 12, Fig. 5b) are not consistent with the earliest lower limiting dates and do not capture the rapid fall suggested by the data. A similar mismatch exists at Mesters Vig (site 13, Fig. 5b). In addition, at this site, a number of late Holocene upper limiting dates suggest RSL was close to present-day sea level at c. 6 ka BP and best-fit predicted sea level at 6 ka BP reaches no lower than 30 m.

Largely, the data from the northeast consist of lower limiting dates so we cannot be sure of their contemporaneous relationship to RSL. At Hvalrosodden and Hovgaard (sites 14 and 15, Fig. 5b) predicted RSL fails to reach above the HML and also fails to plot above some of the early lower limiting dates. The prediction at Blåsø (site 16, Fig. 5b) is broadly consistent with the data but does not produce the expected rate of sea-level fall. The RSL observations are insufficient to show a fall below present-day sea level but c. 100 km northward of this site, archaeological findings suggest a minor late transgression may have happened at Kronprins Eijland (site 17, Fig. 5c) (Hjort, 1997). Here also the prediction does not reach the HML or produce the observed rate of Holocene RSL fall; which is well constrained by upper and lower limiting dates. The data at this site were collected along a broad stretch of coastline (across which there may have been differential isostatic response) and so should be treated with caution.

In the north of Greenland RSL observations from Jurgen Bronlund Fjord (site 18, Fig. 5c) suggest a very rapid fall in sea level at c. 8 ka BP. The prediction for Huy1 shows a very late switch to RSL fall

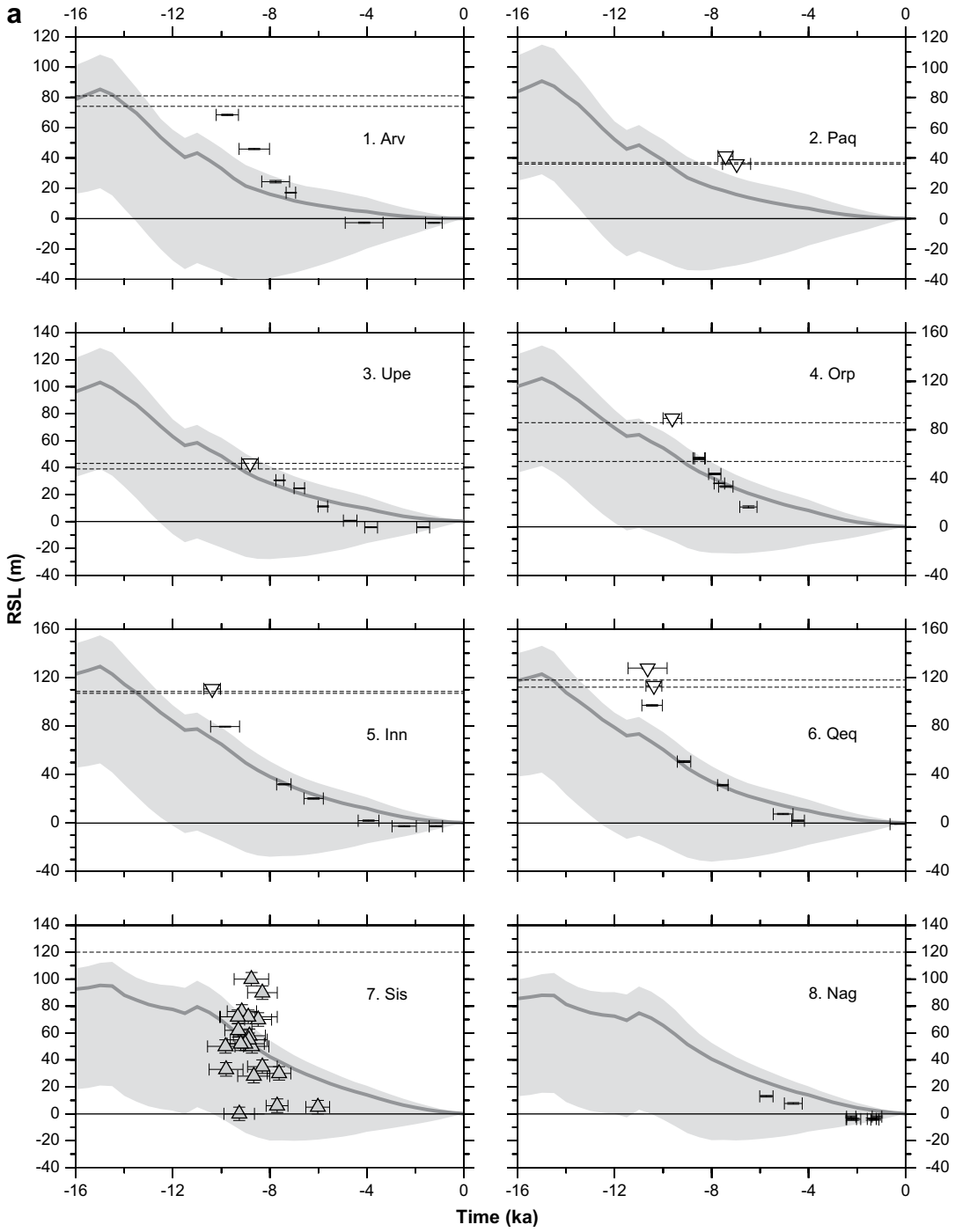

Fig. 5. RSL predictions and observations at the 20 sites considered in this analysis. Predictions, based on the Huy1 ice model and 108 Earth models, fall within the light grey shaded area (see Sub-Section 3.1.1). The dark grey line denotes the RSL prediction for the best-fit Earth model of Huy1; characterised by a 71 km thick lithosphere, upper mantle viscosity of 5×10^{20} Pa s and lower mantle viscosity of 5×10^{21} Pa s (see Sub-Section 3.1.2). Lower limiting dates are shown as grey triangles. Upper limiting dates are shown as inverted white triangles. Sea-level index points are represented by both time and height error bars. The HML at each site is indicated by a horizontal dashed line; if two lines are shown their vertical displacement represents the uncertainty in this value. Qaqortoq (site 9) includes additional observational constraints, indicated by two extra horizontal dashed lines. The line at −8.7 m marks a marine basin that shows no evidence of freshwater incursion and defines a lower bound on RSL change. The line at 39.7 m and traced from 9.5 ka BP to present-day marks the minimum age of deglaciation for a basin and defines an upper bound on RSL change.

when compared to the early data from this site. As a consequence, the best-fit prediction grossly misfits the upper limiting dates that lie close to present-day sea level and are dated to the mid-Holocene.

Across Washington Land in the northwest of Greenland, investigations have shown that the HML declines from c. 100 m in the north to c. 60 m in the southwest (Bennike, 2002). The RSL data are grouped into Lafayette Bugt (site 19, Fig. 5c) and Humboldt Gletscher and Cass Fjord (site 20, Fig. 5c). The sparse time–height coverage of the data in this region means that past RSL change is not well defined. At our final site, the best-fit prediction is inconsistent with some of the older minimum limiting dates (i.e. RSL is too low too early).

We summarise the above discussion with the following conclusions. At seven sites, predicted RSL does not reach the HML

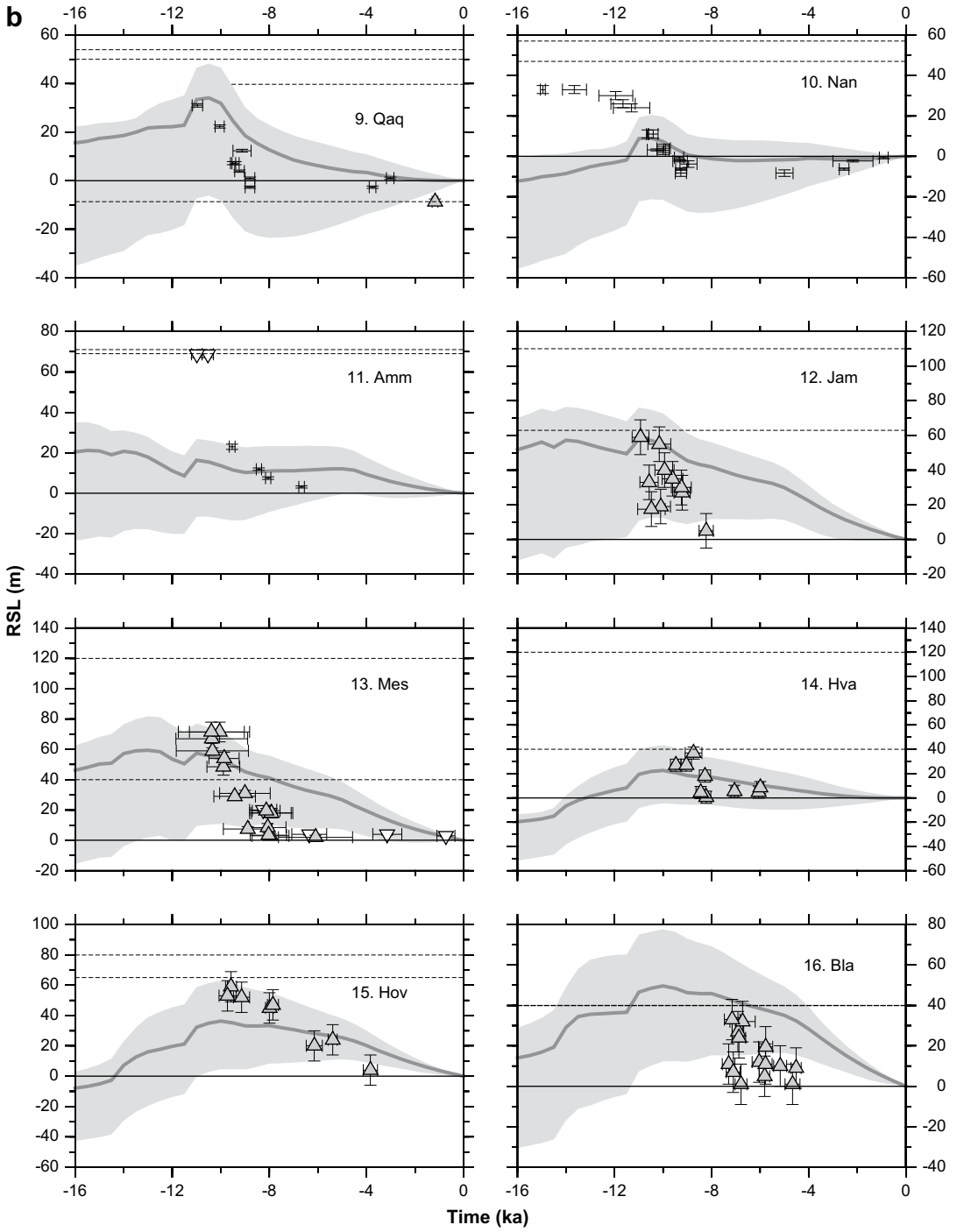

Fig. 5. (*continued*).

(even considering the spread associated with mantle viscosity sensitivity). In west, south (at Nanortalik) and southeast Greenland sea level does not reach high enough to fit the earliest index point data. At the majority of sites the timing of the predicted RSL fall is too early and rate of the fall too slow when compared with the observations. The exception to this is north Greenland where predicted sea-level fall is too late. Observations across Greenland indicate RSL was very close to or even below present-day levels for some part of the Holocene; predicted sea level either does not produce this result or incorrectly produces the timing and magnitude of this fall.

Inspection of the results in Fig. 5 indicates that a significant portion of the data-model misfit cannot be accounted for by varying Earth viscosity parameters within the ranges considered. An important result of our Earth model sensitivity analysis is that the timing of RSL fall at most localities is insensitive to changes in viscosity structure and so must be driven by the ice model. We conclude that the Huy1 model is not capable of providing acceptable fits to the RSL observations for a broad suite of Earth viscosity models. We therefore proceed, in the next section, to address some of these ice model-related misfits by altering key ice model parameters.

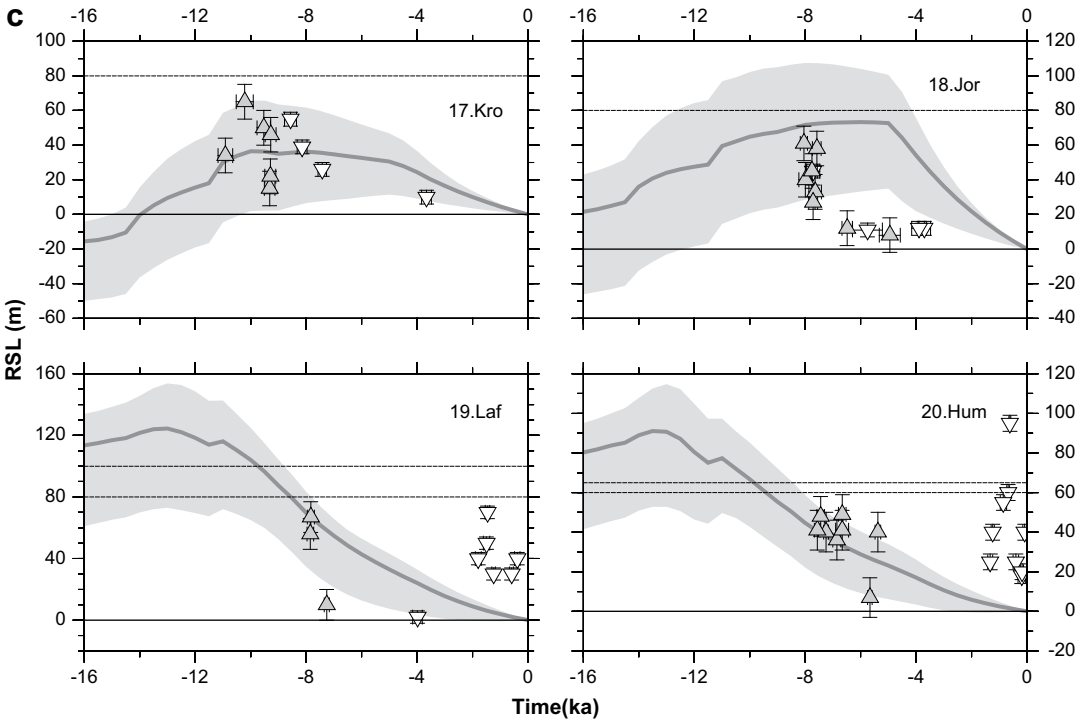

Fig. 5. (*continued*).

3.2. Calibrating the ice model

In the following Sub-Sections (3.2.1–3.2.3) we outline the changes made to the Huy1 model to try and address the data-model misfits discussed above. It is important to note that each change introduced to the Huy1 model is retained and implemented in all following sub-sections. We begin with the LGM extent of the GrIS and then go on to examine two aspects of the ice model forcing: sea level and temperature. We justify and constrain each of these forcings using a combination of both independent evidence and RSL data-model misfits. We demonstrate the sensitivity of the ice model output as well as the RSL response to plausible parameter variations where appropriate.

3.2.1. LGM extent

The maximum extent of the Huy1 model is limited by a mask which acts to confine the growth of the ice sheet across the continental shelf. The mask is based upon sparse evidence of the LGM extent taken from Funder (1989), Funder et al. (1998) and Solheim et al. (1998). The Huy1 mask allows the LGM ice model to reach (approximately) the mid-shelf in the west, the outer shelf in the south and southeast and only the fjord mouths and inner shelf in the east and northeast (Fig. 6). More recent studies, however, are elucidating a pattern of LGM extent that is somewhat larger than these previous findings suggest.

Marine observations from northeast Greenland have produced perhaps the most compelling new evidence. Geophysical surveys and gravity cores taken from the continental margin in this region (the area approximately 72–75°N) indicate that LGM ice extended to the mid-shelf (Wilken and Mienert, 2006) or even to the outer shelf and may have reached the shelf break (O'Cofaigh et al., 2004). Geophysical data have shown a moraine on the mid-shelf, which may define maximum LGM ice extent (Evans et al., 2002), or it is a recessional feature and so marks a post-LGM margin position. Further north, at Nioghalvfjerdsfjorden, Bennike and Björck (2002) suggest that LGM ice may have reached the shelf edge. Whilst at Scoresby Sund, where LGM ice is thought to have reached no further than the fjord mouth (Dowdeswell et al., 1994), recent cosmogenic dates suggest that in east Greenland LGM ice may have also reached to the outermost shelf (Håkansson et al., 2007). These recent findings are in contrast to the coastal position of LGM ice extent defined by the mask of Huy1 for northeast and east Greenland. The continental shelf is wide and shallow in the northeast and so the changes suggested by these new observations are significant (e.g. compare grey and black dashed lines in Fig. 6). If the ice margin was positioned on the outer shelf rather than the coast we would expect a marked difference in LGM ice load over this region.

In southeast Greenland radiocarbon dates from the shelf adjacent to the Kangerlussuaq outlet glacier (Jennings et al., 2006) imply LGM ice terminated near the shelf break (also see a review of the evidence by Andrews (2008)). Farther south and close to the Helheim outlet glacier, new cosmogenic exposure ages (Roberts et al., 2008) and other radiocarbon dates from the shelf similarly indicate that the ice margin was at or close to the shelf break (Kuijpers et al., 2003). Moreover, a GIA modelling study constrained by new RSL data from Ammassalik has shown that the LGM position of the Huy1 model is insufficiently extended onto the shelf in southeast Greenland (Long et al., 2008). Similar modelling studies in south Greenland have found that the LGM ice margin reached the shelf break (Bennike et al., 2002; Sparrenbom, Ph.D. thesis). Across west and southwest Greenland there are no new observations to challenge or validate the traditional model of LGM extent as reflected in the Huy1 mask. Two distinct moraine systems have been identified on the inner and outer shelf in this region (Brett and Zarudzki, 1979). Kelly (1985) uses the height of a nunatak moraine system in southwest Greenland to infer that the ice margin terminated on the inner shelf. Other moraine systems from south Disko (Ingolfsson et al., 1990) are interpreted as LGM extent, although it cannot be ruled out that these mark a readvance or are recessional features (Weidick and Bennike, 2007).

The current evidence is insufficient to precisely define the LGM position of the ice margin across Greenland. Given this

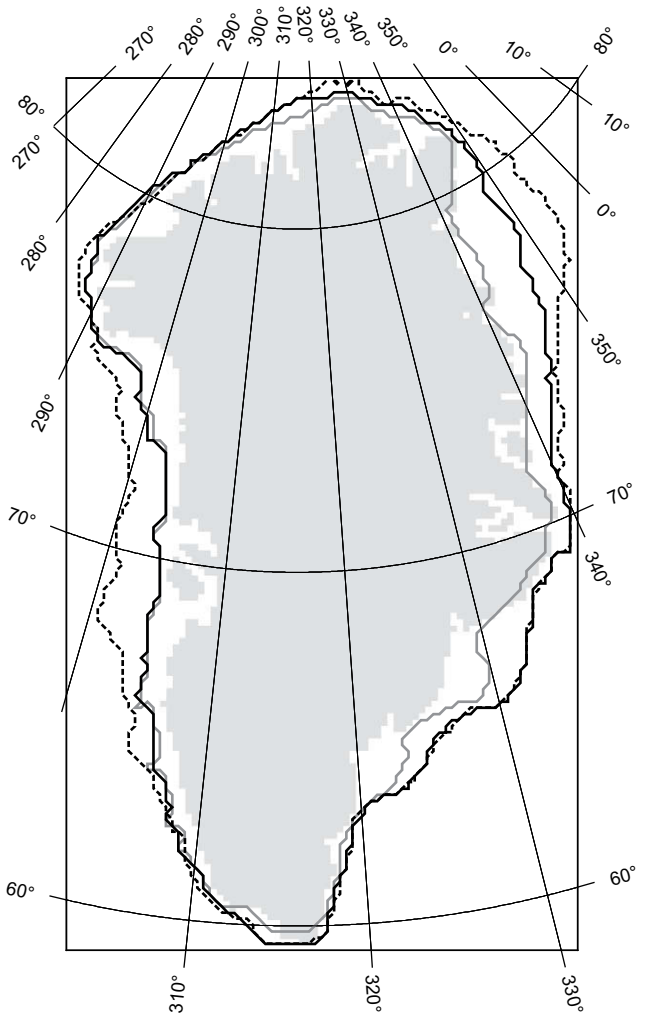

Fig. 6. The three LGM ice mask extents considered in this analysis: the original mask of Huy1 (solid grey); the shelf break mask (black dashed; which roughly coincides with a 400 m bathymetric depth) and our chosen (hybrid) mask (solid black). See main text for more information. Modelled present-day coastline is shaded light grey.

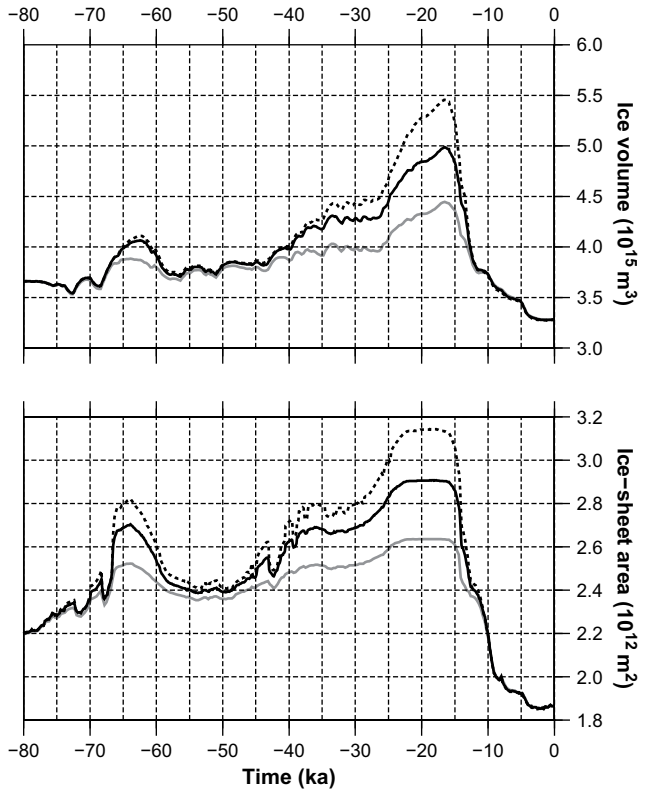

Fig. 7. Ice sheet volume and extent changes for the three different LGM extent scenarios shown in Fig. 6: shelf break (black dashed), our chosen (hybrid) LGM extent (solid black) and Huy1 mask (solid grey).

uncertainty, it is appropriate to examine the sensitivity of RSL predictions to a small suite of plausible LGM ice margin configurations to see if some of the misfits discussed above can be reconciled through this aspect of the ice model. We introduce two alternative masks that delimit the LGM ice extent. The first allows the ice sheet to expand, if in positive mass balance, to the shelf break (dashed black line – Fig. 6). The second mask is a hybrid scenario that most closely reflects the new geomorphological and modelling evidence outlined above (solid black line – Fig. 6). This allows the ice sheet to expand to the mid-to-outer shelf in the northeast, the shelf edge from east to south Greenland and follows the original Huy1 mask elsewhere. Even though there remains considerable uncertainty in the LGM extent of the ice sheet, we consider this hybrid scenario as the most accurate at this time. We note that in each case the ice model grows to completely cover the area defined by the mask.

We show, in Fig. 7, the modelled ice volume and spatial extent for the past 80 ka BP based on the three LGM masks introduced above. These results indicate that there are large differences in LGM volume and spatial extent for the different scenarios considered. For example, the Huy1 model predicts 2.7 m excess ice-equivalent sea level at the LGM, compared to 5.2 m for the maximum (shelf break) extent model and 4.1 m for our preferred hybrid model.

The sea-level predictions generated from the three LGM extent scenarios considered are illustrated for eight representative RSL sites in Fig. 8 (note that the colour and style of the lines shown correspond to those in Figs. 6 and 7 for a given LGM mask). In general (and unsurprisingly) we find the largest differences in the RSL response where the distances between the masks are largest. For northeast Greenland where the shelf is at its widest and the original Huy1 mask hugs the coastline, there is a c. 100 m difference between RSL predictions at 10 ka BP for Hovgaard (site 15, Fig. 8). The comparison was made at 10 ka BP because this is when the largest discrepancy occurs during the period that observational constraints exist at this site. Using this same approach in south Greenland, the RSL response at 15.5 ka BP for Nanortalik (site 10, Fig. 8) varies by c. 20 m. Here the shelf is narrow c. 30–60 km and so the differences between the masks are relatively small.

Changes to the LGM mask do not influence the timing of predicted RSL fall; a similar finding as from our Earth model sensitivity analysis. Our preferred LGM hybrid mask is most different to the original Huy1 mask in southeast, east and northeast Greenland. Here our preferred hybrid mask generally predicts higher RSL and a more rapid RSL fall. The revision of the mask improves the data-model fit for northeast Greenland where lower limiting observations now show fit to predicted RSL for our reference Earth model. For southeast Greenland predicted sea level now reaches to the HML. But in both the southeast and east, however, the observations still indicate that RSL fall is mistimed and/or the rate of RSL fall is too low. For areas where the mask is little changed or its position not revised the data-model misfits described in Section 3.1.3 remain.

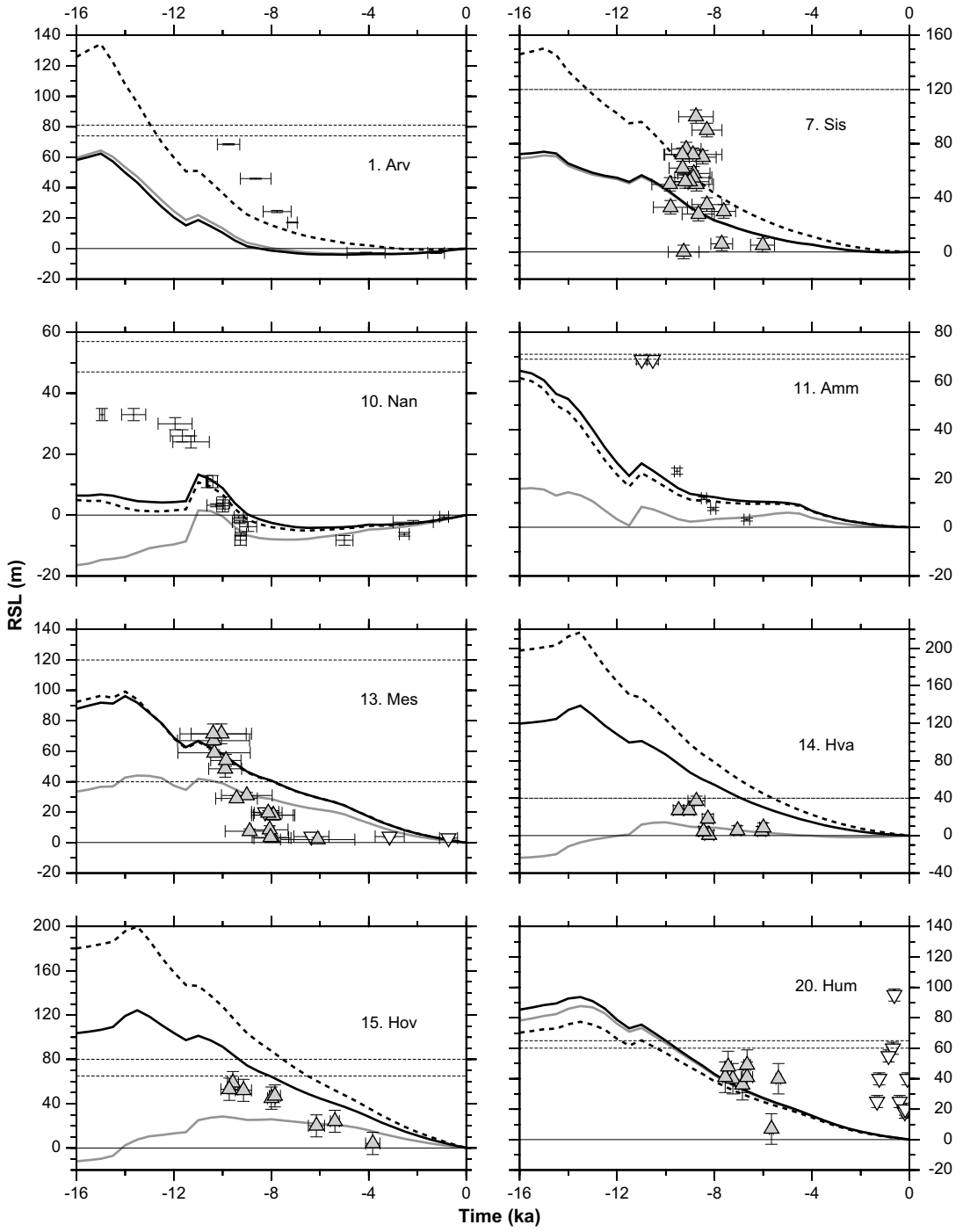

Fig. 8. The influence of LGM extent on the sea-level predictions for our reference Earth model. The shelf break (black dashed), our chosen mask (solid black) and original Huy1 mask (solid grey). Lower limiting dates are grey triangles. Upper limiting dates are inverted white triangles. Sea-level index points are represented by both time and height error bars. The HML at each site is indicated by a horizontal dashed line; if two lines are shown their vertical displacement represents the uncertainty in this value.

3.2.2. Sea-level forcing

At present there is no reliable way to simulate the grounding-line (Vieli and Payne, 2005) or the position of the calving front if there is no ice shelf. The application of simple marine parameterisations has been shown to successfully reproduce first-order ice margin changes in areas below sea level (Zweck and Huybrechts, 2003, 2005). The sea-level forcing of Huy1 uses an empirical formulation that parameterises the maximum grounding depth of the ice sheet (H_c) as a function of eustatic sea-level change (ΔH_{sl}):

$$\begin{aligned} H_c &= -0.25 \times (\Delta H_{sl} + 80)^2 + 2\Delta H_{sl} \text{for} \Delta H_{sl} < -80m, \\ H_c &= 2\Delta H_{sl} \text{for} \Delta H_{sl} > -80m \end{aligned} \quad (2)$$

This assumes that water depth is the sole control on the extent of the marine margin and that beyond the maximum grounding depth all ice is calved. It should be noted that the eustatic sea-level record (ΔH_{sl}) used in Huy1 is derived from the SPECMAP stack of marine oxygen-isotope values (Imbrie et al., 1984). The empirical

relationship, given in Eq. (2), is hybridised to reproduce the advancement of the ice sheet over the continental shelf. During times of low eustatic sea level this relationship allows the ice sheet to expand onto the continental shelf and reach the maximum margin extent (as defined by the mask). Conversely, rising eustatic sea level will force the ice margin landward.

Observational evidence on the timing of ice margin retreat across the continental shelf is generally limited. In northeast Greenland retreat commenced after c. 18 ka BP and had abandoned the inner shelf by c. 14.6 ka BP (Evans et al., 2002). The beginning of deglaciation is dated to c. 18.6 ka BP in east Greenland (Nam et al., 1995). In southeast Greenland dates from the cross-shelf Kangerlussuaq trough suggest the GrIS remained near to the shelf edge until 17 ka BP (Mienert et al., 1992). Other dates from the trough indicate the mid-shelf became ice-free c. 16–15 ka BP (Smith and Licht, 2000; Jennings et al., 2002, 2006). Just south of Ammassalik (site 11) another marine core study shows ice margin retreat in this area occurred shortly before c. 15 ka BP (Kuijpers et al., 2003). The timing of marine retreat in other areas of Greenland is less well known; in west Greenland the deglaciation of the main part of Disko Bugt was dated to a minimum of 10.2 ka BP (Long et al., 2003; Lloyd et al., 2005) but less is known about the shelf west of Disko Island.

Given the remaining uncertainty in margin retreat across the shelf in many areas, we follow the procedure adopted in the previous sub-section and construct a small number of plausible but contrasting retreat scenarios. We make changes to the marine extent parameterisation knowing that (1) the ice model must be allowed to reach its newly defined maximum extent at LGM and (2) the ice sheet had essentially retreated from the continental shelf by c. 10 ka BP (Funder and Hansen, 1996; Bennike and Björck, 2002). We apply three different parameterisations of Eq. (2) to consider three different shelf retreat scenarios. The first is a simple linear relationship between maximum grounding depth and eustatic sea-level change:

$$H_c = 10.27 \times (\Delta H_{sl} + 52) \text{ for } \Delta H_{sl} \leq -52m,$$
$$H_c = 0 \text{ for } \Delta H_{sl} > -52m \quad (3)$$

The second produces an early retreat leaving large parts of the shelf ice-free by 14 ka BP – this forcing creates a similar pattern of recession as the original sea-level forcing of the Huy1 model:

$$H_c = -0.185 \times (\Delta H_{sl} + 80)^2 + 5.14 \times (\Delta H_{sl} + 52) \text{for} \Delta H_{sl} \leq -80m,$$
$$H_c = 5.14 \times (\Delta H_{sl} + 52) \text{ for } -80 < \Delta H_{sl} < -52m,$$
$$H_c = 0 \text{ for } \Delta H_{sl} \geq -52m \quad (4)$$

The third sea-level forcing produces a relatively late (c. 12 ka BP) and very rapid retreat of the ice margin:

$$H_c = 6\Delta H_{sl} \text{ for } \Delta H_{sl} \leq -80m,$$
$$H_c = 0.398 \times (\Delta H_{sl} + 80)^2 + 6\Delta H_{sl} \text{ for } -80 < \Delta H_{sl} < -52m,$$
$$H_c = 0 \text{ for } \Delta H_{sl} \geq -52m \quad (5)$$

In each case the marine retreat does not begin until after 16 ka BP. Further, in all experiments we prescribe the hybrid mask as detailed in the previous sub-section. The resulting GrIS extent changes for each scenario are shown in Fig. 9.

On inspection of Fig. 10, it is clear that the changes made to the sea-level forcing exert a strong control on the predicted timing of the initial RSL fall (note that the colour and style of the lines shown correspond to those in Fig. 9 for a given sea-level forcing). The difference in this timing is most pronounced in areas where the continental shelf is flat and wide and/or there is the presence of cross-shelf troughs. In these areas a small change in the allowed maximum grounding depth of the ice sheet (H_c) can result in a very large migration of the modelled ice margin. In southeast Greenland at Ammassalik (site 11, Fig. 10) the timing of initial predicted RSL fall shows a c. 5 ka difference depending on the sea-level parameterisation implemented. Ammassalik sits close to the entrance of the Helheim outlet glacier and its associated cross-shelf trough. The trough is deeper than the surrounding continental shelf and therefore rapidly calves ice once the ice margin reaches its edge. Whereas in south Greenland at Nanortalik (site 10, Fig. 10), where the shelf is narrow, the timing of initial RSL fall shows little sensitivity to changes of the sea-level parameterisation.

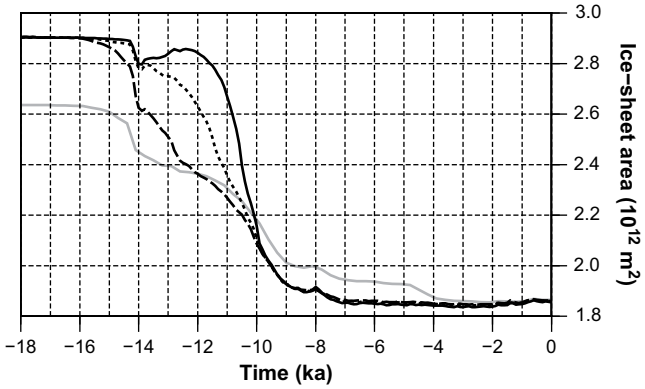

Fig. 9. Ice sheet extent changes for four different sea-level forcing scenarios: original Huy1 model (solid grey), linear retreat from shelf (dotted black), early retreat (dashed black), and late retreat (solid black). Note that the predictions shown in black include the optimum LGM extent discussed in Section 3.2.1.

Across west (site 1), southwest (site 7) and arguably southeast Greenland (site 11) the RSL data favour a relatively late and rapid retreat from the shelf (Fig. 10). The timing of predicted RSL fall from the HML is in better agreement with the sea-level data from these regions. If LGM ice terminated on the inner shelf in west Greenland then we suggest retreat initiated c. 12 ka BP. Elsewhere in Greenland the picture is less clear: with poorer quality limiting dates it is difficult to discriminate between the different parameterisations as in some cases they all provide an adequate fit (e.g. Hovgaard, site 15). If the limiting dates do correspond closely to past mean sea level, then RSL data from the east and northeast could be interpreted as favouring the earlier retreat scenario. Care must be taken when using RSL observations alone to discriminate between the different forcing scenarios due to the sensitivity of the predictions to other poorly known input parameters (e.g. Earth viscosity structure). However, the independent observational evidence discussed above suggests a relatively early deglaciation down the entire east coast of Greenland. As different retreat scenarios are favoured in different regions of Greenland then it indicates the pattern of retreat is not well produced by the model. It is also possible that these differences reflect changes in lateral Earth structure and rheology (see Sub-Section 4.3.3). Further, we note that the sea-level parameterisation considers the maximum grounding depth to be a function of the eustatic signal and the expected pattern of sea-level change across Greenland would likely depart significantly from this. Changes to the sea-level parameterisation will only alter the timing of the marine retreat; the spatial pattern of retreat from the continental shelf will remain fairly uniform. Given this, we opt for the relatively late deglaciation scenario as this gives best-fit to the highest quality RSL data from west, southwest, south and southeast Greenland.

Across southwest, south and southeast Greenland we find that the retreat from the shelf is not continuous: the ice model undergoes a marine retreat and subsequent readvance from 14 to 12 ka BP (Fig. 11) This change indicates that, over this period, the migration of the modelled ice margin is being driven by mass

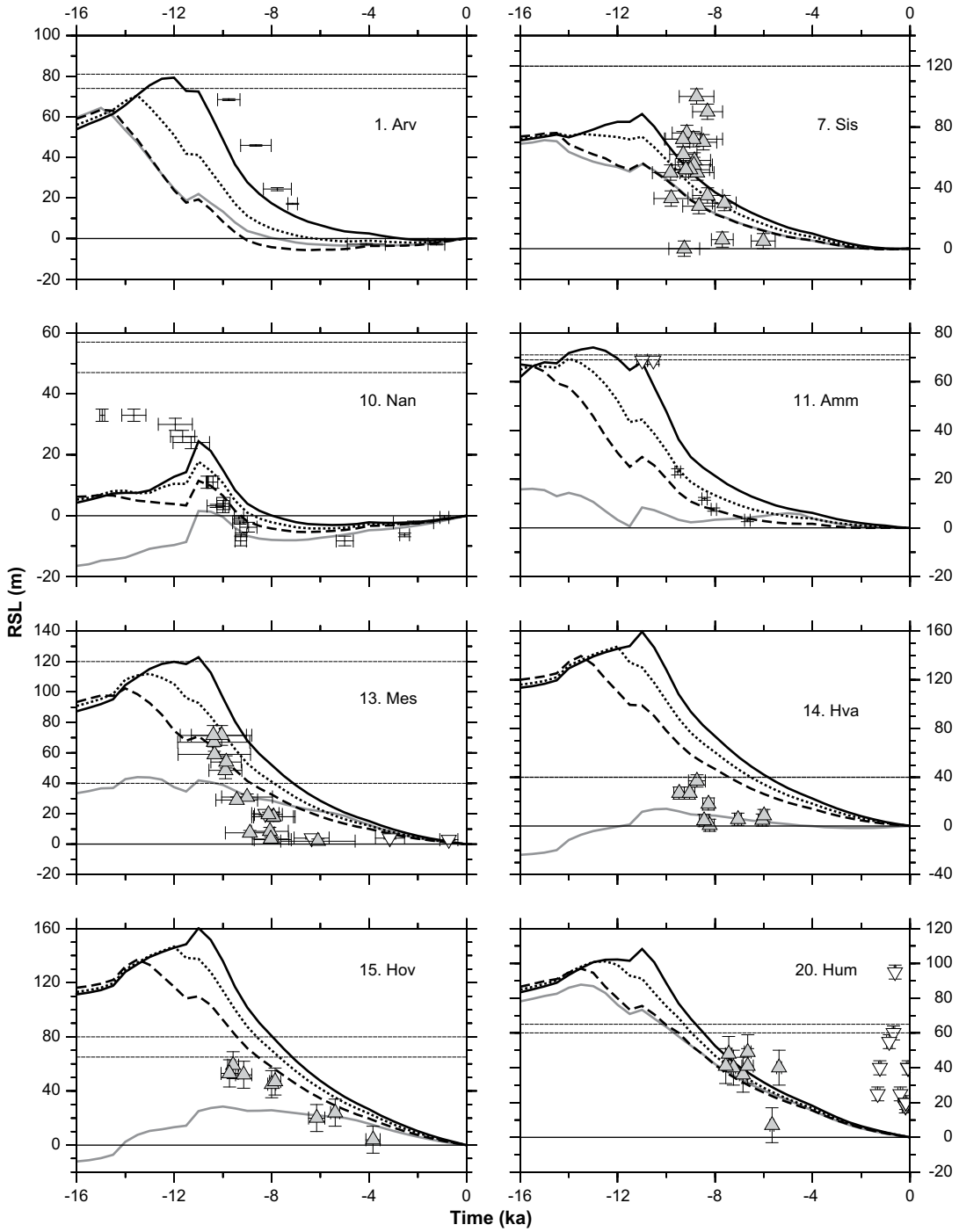

Fig. 10. The influence of different sea-level forcing parameterisations on the sea-level predictions for our reference Earth model. The linear parameterisation (dotted black), the relatively early marine retreat (dashed black), relatively late retreat (solid black) and Huy1 model (solid grey). Upper limiting dates are inverted white triangles. Sea-level index points are represented by both time and height error bars. The HML at each site is indicated by a horizontal dashed line; if two lines are shown their vertical displacement represents the uncertainty in this value.

balance changes rather than sea-level rise (this is also evident from the departure of the dark blue from the red line in Fig. 13). The initial retreat of the ice margin can be correlated to Bolling–Allerod (c. 14 ka BP) warming whilst the subsequent readvance marks the transition to the Younger Dryas (YD, c. 11.5 ka BP) cold period. This suggests that any sign of an YD readvance of the ice sheet margin would have been recorded on the continental shelf in the southern sectors of Greenland. Evidence for this can be found in south Greenland where Weidick et al. (2004) argue that the Neria stade records an ice sheet readvance on the inner shelf that occurred shortly before 11 ka BP. Weidick et al. (2004) note that past interpretation of the Neria stade is of LGM age (Kelly, 1985) and that LGM ice extent in west Greenland was similarly interpreted and therefore the chronology there requires similar revision.

3.2.3. Temperature forcing

The Huy1 ice model is forced using temperature changes inferred from the GRIP $\delta^{18}O$ ice core record (Dansgaard et al., 1993).

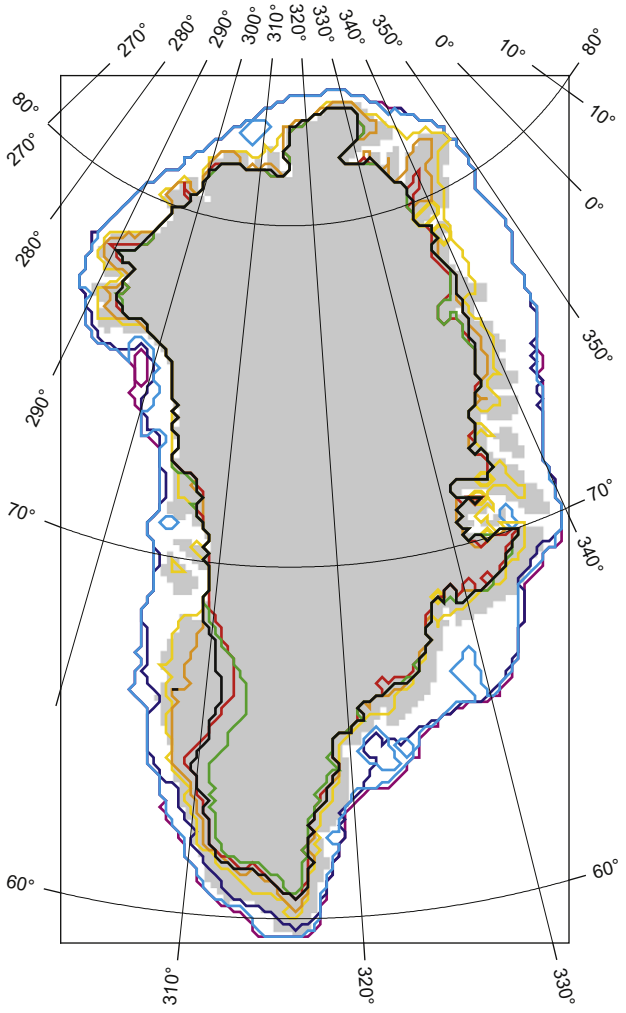

Fig. 11. Modelled ice margin chronology for the new Huy2 model; pink – 16 ka BP, dark blue – 14 ka BP, light blue – 12 ka BP, yellow – 10 ka BP, orange – 9 ka BP, red – 6 ka BP, green – 4 ka BP (minimum extent) and black – present-day. Modelled present-day coastline is shaded dark grey.

The transformation from $\delta^{18}O$ to a temperature record (ΔT) (Eq. (6)) is dependent on a conversion factor (d) and is corrected for elevation changes that occur at the ice core site (ΔT_E):

$$\Delta T(t) = d\left(\partial^{18}O(t) + 34.83\right) - \Delta T_E(t). \quad (6)$$

The conversion factor (d) is equal to the inverse of the climatic isotopic sensitivity (as described in Cuffey (2000)) and taken as a constant. The transformation does not take into account the influence of elevation changes on the climatic isotopic sensitivity. Such changes may well be important over periods of small temperature change (Huybrechts, 2002). This may explain why the temperature forcing of Huy1 shows little evidence of warming over the Holocene period (Fig. 12).

Temperature profiles obtained from ice borehole studies are able to resolve Holocene surface air temperature change at the GRIP and Dye3 sites (Dahl Jensen et al., 1998) and they indicate that the HTM at summit (GRIP) had an amplitude of 2.5 °C (all temperatures are relative to present-day) and that it was 1.5 times warmer to the southwest (Dye3). Another ice core study from summit Greenland (GISP2) indicates a smaller amplitude HTM (Cuffey et al., 1995). To the north of Greenland the amplitude of the HTM is observed to be 2 °C at the Agassiz Ice Cap on Ellesmere Island in the Canadian

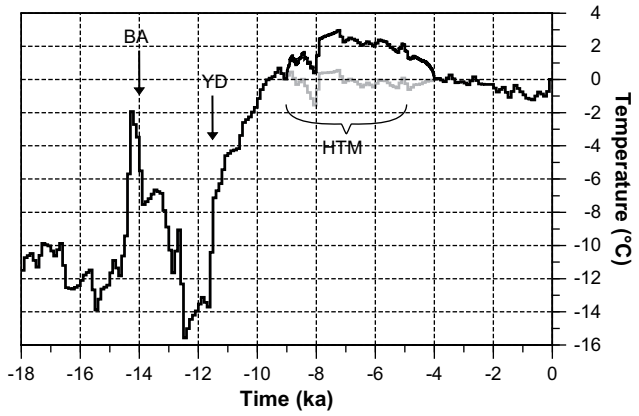

Fig. 12. The Huy1 temperature record (grey) and our revised temperature forcing with imposed Holocene thermal maximum (black) at the GRIP site. Spatial changes made to the temperature forcing over the Holocene thermal maximum are outlined in the text. Annotations show the climatic events of the Bolling–Allerod (BA, c. 14 ka BP), Younger Dryas (YD, c. 11.5 ka BP) and Holocene Thermal Maximum (HTM, c. 9–5 ka BP).

Arctic (Koerner and Fisher, 1990). Given the clear and widespread evidence for the HTM, we superimpose a parabolic warming to the original temperature forcing of Huy1 so that the above data constraints are broadly reproduced. At GRIP the imposed amplitude of warming is 2.5 °C and increases linearly with decreasing latitude to reach a value 1.5 times larger at the Dye3 site (the forcing remains fixed south of this). North of GRIP the forcing is decreased linearly with latitude to the site of the Agassiz Ice Cap where it has a value of 2 °C. We also consider results from Kaufman et al. (2004) (see their Fig. 7) to constrain the spatial and temporal pattern of the HTM in Greenland. Much of the evidence described comes again from borehole studies (Dahl Jensen et al., 1998) that indicate that the HTM peaked during the period 8–5 ka BP at GRIP and between 6 and 3 ka BP at Dye3. Other palaeoenvironmental evidence from lake cores and terrestrial archives supports the finding that warming is generally thought to have occurred later in south Greenland (e.g. Kaplan et al., 2002). In northwest Greenland, warming at the Camp Century site is thought to have occurred between 8 and 4 ka BP (Dansgaard et al., 1971) with similar timing (at least when considering millennial-scale changes) found in the northeast (Bennike and Weidick, 2001). The duration of the imposed HTM changes linearly between 8 and 4 ka BP in the north, 8 and 5 ka BP at summit to 6 and 3 ka BP in the south. Fig. 12 illustrates the temperature record at summit Greenland (GRIP) as implemented for Huy1 (grey line) and for our revised record that includes an imposed HTM (black line).

The Huy1 model is tuned to fit the adapted (P. Huybrechts, personal communication) observations of present-day ice sheet elevation and thickness of Bamber et al. (2001). Given our new imposed HTM warming, the modelled present-day ice sheet elevation and thickness now differs from both the Huy1 model and the present-day observations. As part of the ice model's melt- and runoff treatment (Braithwaite, 1995; Janssens and Huybrechts, 2000); degree day factors (DDFs) are used to calculate the amount of meltwater, eventually leading to runoff after saturation of the snowpack. The DDFs are applied uniformly and for snow and ice melting are 3 and 8 mm/day/°C (water equivalent), respectively. We therefore make gradual changes to the DDFs over the Holocene period to ensure the present-day ice sheet is produced as closely as possible (Fig. 13). The DDFs are reset to their original values over the last few thousand years so that the model evolves to its present-day reference state and therefore matches the modelled present-day volume and extent of Huy1 (which is tuned to fit the observed ice sheet). We find that a reduction of the DDFs by 30% over the

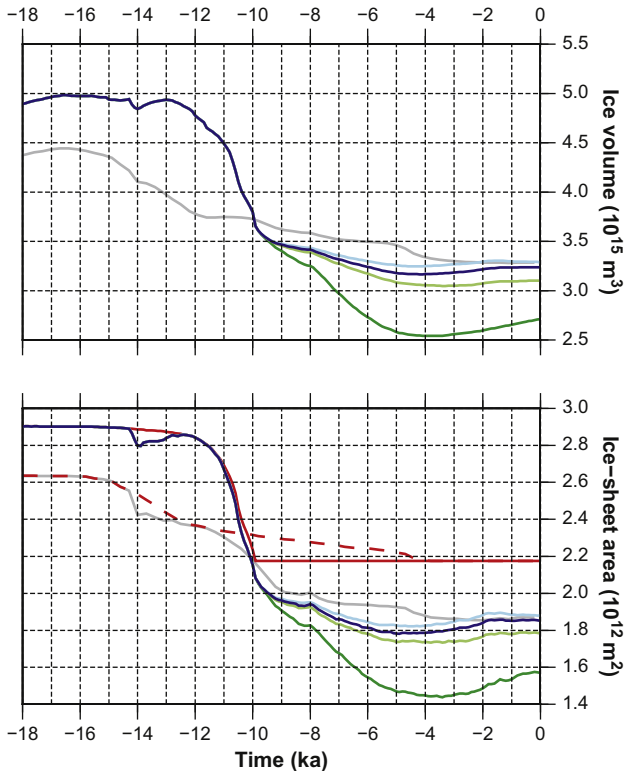

Fig. 13. Predictions of ice sheet volume and extent for the revised temperature forcing. Changes are made to the degree day factors to obtain agreement with the observed present-day GrIS. Changes to the degree day factors are 0% (dark green), −25% (light green), −30% (dark blue – which represents the best-fit) and −35% (light blue). Note that the predictions shown include the optimum LGM extent mask and sea-level forcing discussed, respectively, in Sections 3.2.1 and 3.2.2. The evolution of the Huy1 model is shown as grey. The maximum allowed ice extent as defined by the LGM mask and sea-level forcing is shown for Huy1 (dashed red) and the new ice model (red).

mid-Holocene gives the best-fit to the present-day observations. This change to the DDFs is within the typical uncertainty on these model parameters as inferred from direct ablation measurements (Braithwaite, 1995).

The influence of the imposed HTM on the sea-level predictions is shown in Fig. 14 (compare dotted and solid black lines). It should be noted that for this experiment we prescribe the relatively late deglaciation (c. 12 ka BP) and hybrid mask as detailed in the previous sub-sections. In regions where the ice margin has a larger response to the increased HTM warming we find the RSL curve is lowered over the mid-late Holocene. RSL data from west, southwest and south Greenland are well constrained over this time period. As a result of the imposed warming, predicted mid-Holocene RSL (using our reference Earth model) in west Greenland falls below present-day levels and is in better agreement with the data. The data-model fit is also improved for both southwest and south Greenland; bringing the curve lower and nearer the index point data situated below present-day sea level. We note that RSL predictions are shown relative to present-day sea level, which is why the RSL curve intercepts the y-axis at zero height. This means that imposing a HTM that changes both Holocene and present-day predicted sea level will also impact predictions at earlier times (note differences in the dotted and solid black lines prior to 9 ka BP).

3.3. Sea-level predictions based on the Huy2 model

In this section, we adopt the new ice model resulting from the revisions described in Section 3.2 (hereafter referred to as Huy2) and compare the RSL data to predictions at all of the data sites.

3.3.1. Determining an optimal viscosity model

We computed model predictions for the Huy2 model using the suite of Earth viscosity models described in Sub-Section 3.1.1. Comparing these predictions to the data gives the χ^2 values shown in Fig. 15. Comparison of these results to those of Huy1 (shown in Fig. 4), demonstrates that the Huy2 model gives an improved data-model fit. Additionally, it indicates that the class of viscosity models providing good fits with the Huy2 ice model is distinct from those identified for the Huy1 model. For example, Earth models with a 71 km thick lithosphere no longer produce the best-fits; the minimum χ^2 values are obtained by models with a 96 or 120 km thick lithosphere. For the 96 km lithosphere model there is a large zone that indicates fit to the data. This is an unsurprising result given that we have been largely focussing on and trying to reduce misfits between RSL observations and sea-level predictions generated using our reference Earth model. The 120 km lithosphere panel shows that the observations favour small values for the lower mantle viscosity and are generally insensitive to upper mantle viscosities. For Huy2 the best-fit model is a 120 km lithosphere with an upper mantle viscosity of 5×10^{20} Pa s and a lower mantle viscosity of 10^{21} Pa s. We note that a model with a 96 km lithosphere, upper mantle viscosity of 5×10^{20} Pa s and a lower mantle viscosity 5×10^{21} Pa s (close to our reference model) gives almost the same fit so we cannot discriminate between these two Earth models.

3.3.2. Comparison of Huy2 model to RSL observations

In Fig. 16 we compare predictions for the Huy2 model to data at all sites considered in this analysis. We show the envelope of predictions for the suite of Earth models discussed above (indicated by dashed black lines) and isolate the prediction based on the best-fit 120 km lithosphere model established in the previous sub-section (solid black line). For comparison, we also show the equivalent predictions for the Huy1 model (as shown in Fig. 5). A visual inspection of the envelope generated using the Huy2 model shows that across Greenland the data-model misfit has been reduced and, in general, sea-level data lie inside and give fit to the envelope. In the following, we address regional data-model fits of the Huy2 model, with focus on the best-fit result and implications for regional ice histories. Given that constraining a GIA model with RSL data is a non-unique inversion problem, we discuss crucial parameter trade-offs and further examine the independent observational evidence that can help reduce this inherent ambiguity. Further, we compare our results with other modelling work (here on a regional scale and with overall results in Section 4).

Across west Greenland (sites 1–6, Fig. 16a), we find that the Huy2 best-fit prediction gives excellent fit to the majority of index point data; although, as discussed above, the χ^2 results are biased toward this part of the dataset and so this is not a surprising result. The central west coast of Greenland is the location of the Jakobshavn Isbrae ice stream that drains c. 7% of the GrIS (Bindschadler, 1984) into Disko Bugt. It is well accepted that Disko Bugt was covered by ice at the LGM (Kelly, 1985; Funder, 1989; Funder and Hansen, 1996; Weidick and Bennike, 2007) and likely housed a predecessor of the Isbrae. There are also suggestions of a late ice shelf west of Disko prior to the last deglaciation (Bennike et al., 1994). Our modelling results imply that if the LGM ice margin did terminate on the inner shelf then the onset of deglaciation appears to be relatively late, starting c. 12 ka BP, followed by a very rapid retreat leaving the embayment ice-free by c. 10 ka BP (Fig. 11). In a previous interpretation of the sea-level data, Long and Roberts (2003) hypothesised that the Isbrae was able to survive the high rates of eustatic sea-level rise and remain on the shelf west of Disko Bugt because of its high rate of ice discharge and the shallow water depths. The subsequent rapid retreat may well be a consequence of

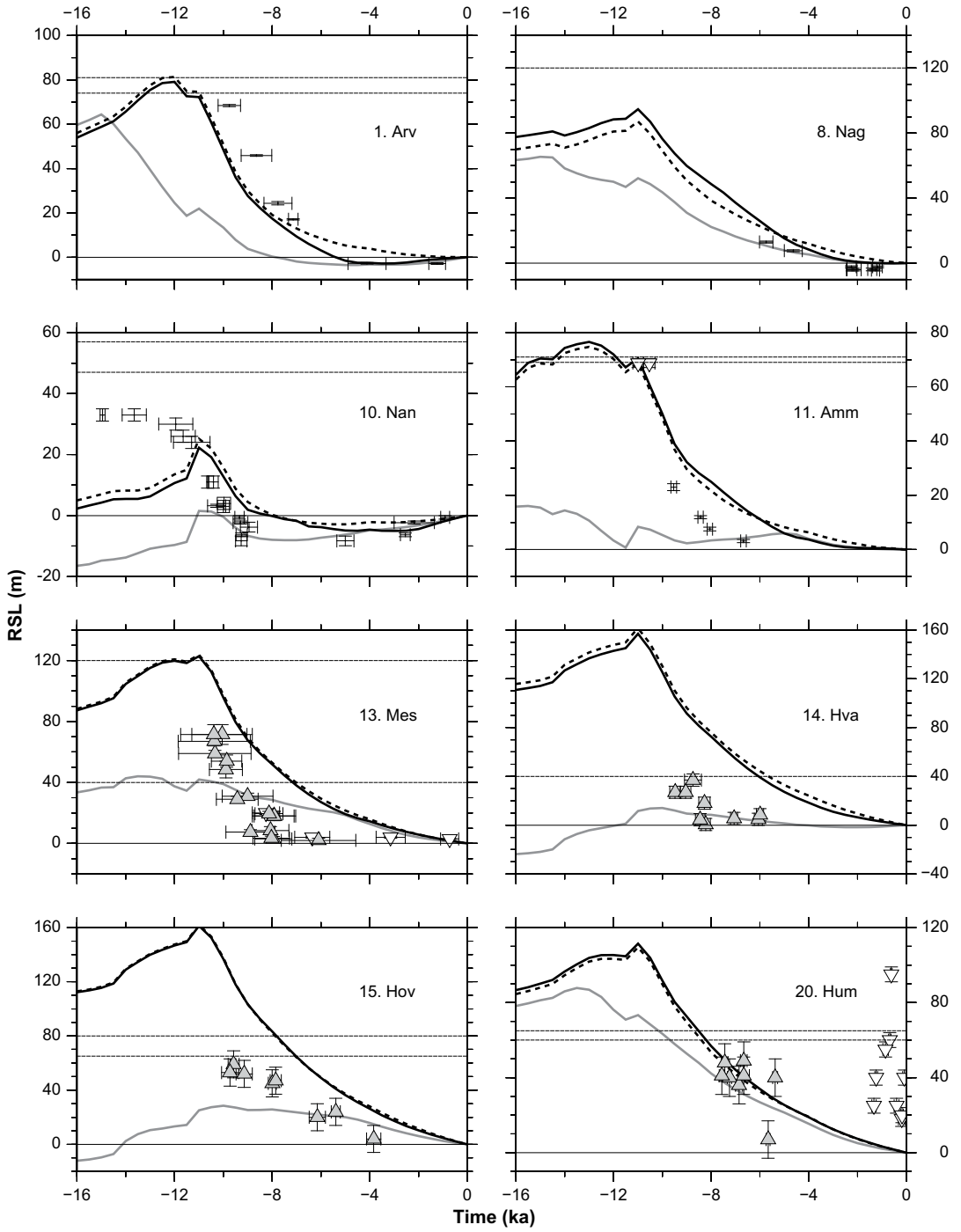

Fig. 14. RSL predictions at selected sites based on our standard Earth model and three different ice models: one that includes a HTM (solid black; see main text for details), one that does not (dotted black) and the original Huy1 model (solid grey). Note that the predictions indicated by the solid black and dashed black lines include the optimum LGM extent mask and sea-level forcing discussed, respectively, in Sub-Sections 3.2.1 and 3.2.2. Upper limiting dates are inverted white triangles. Sea-level index points are represented by both time and height error bars. The HML at each site is indicated by a horizontal dashed line; if two lines are shown their vertical displacement represents the uncertainty in this value.

the large bedrock trough that runs out of the entrance of Disko Bugt. Models of tidewater glaciers, supported by observations, have shown that changes in the bedrock topography are the dominant control on such episodes of rapid retreat (e.g. Vieli et al., 2001; Schoof, 2007).

The Sisimiut data (site 7, Fig. 16a) capture the broad sea-level changes over the early Holocene in southwest Greenland. The best-fit prediction does not reproduce these RSL changes well: the predicted sea-level fall is too gradual and the early-Holocene predicted RSL values are generally too low. However, the upper bound of the predicted envelope indicates that the majority of lower limiting data could be fitted. Nearby at Nagtoralinguaq (site 8, Fig. 16a) the best-fit prediction does not produce the expected late Holocene fall below present-day sea level. The ice margin is known to respond to even moderate warming due to the low accumulation and low altitudes that characterise this region (Letréguilly et al., 1991). Presently the southwest contains the largest area of ice-free land in Greenland across which observational evidence of the

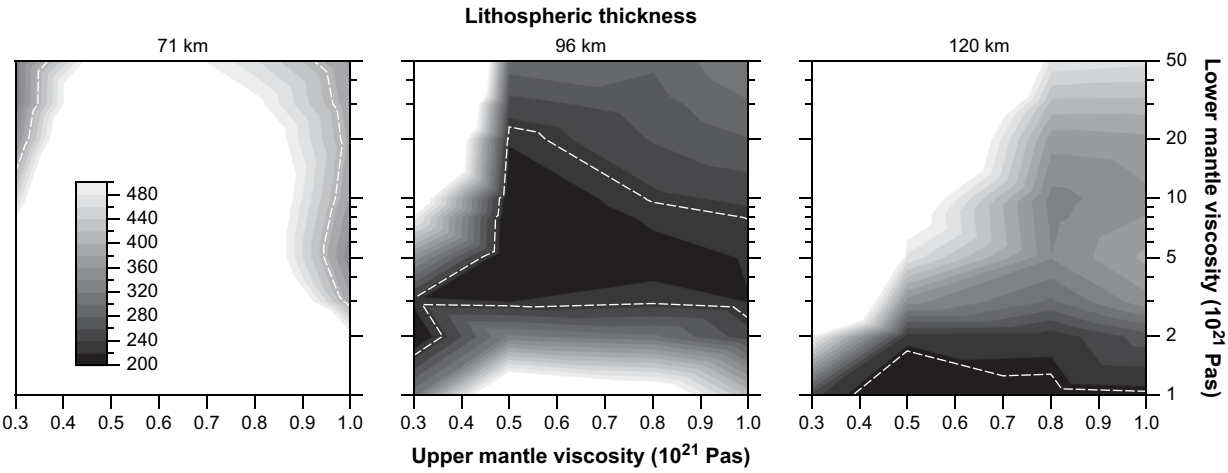

Fig. 15. The Chi-squared results for the Huy2 ice model. The scale bar for the Chi-squared results is shown how in the left-hand frame. The 95% confidence level is marked by the white dashed line.

Holocene retreat is well recognised. Previous ice modelling studies compared with dated recessional moraine systems show there was a fairly continuous Holocene retreat (Van Tatenhove et al., 1995) and the ice margin was behind the present-day margin after c. 6 ka BP (Van Tatenhove et al., 1996). This is in reasonable agreement with ice history of the Huy1 and Huy2 models; Huy2 retreats behind the present-day margin in southwest Greenland between 7 and 6 ka BP (Fig. 11 shows the 6 ka BP ice margin). The GrB Greenland model of Tarasov and Peltier (2002) shows a good fit to the Inner and Outer Søndre Strømfjord RSL data (Ten Brink and Weidick, 1974) from southwest Greenland but differs from Huy1 and Huy2 in its Holocene evolution; at 10 ka BP the modelled ice margin is at the coastline and by 8 ka BP has retreated well inland of its present-day position to reach its minimum state. After this time, GrB undergoes a readvance in southwest Greenland; comparison of predictions from the ICE-5G model to recent geodetic measurements suggests that this readvance is too large or mistimed (Khan et al., 2008).

In south Greenland the Huy2 best-fit model shows little improvement on the Huy1 results. For Nanortalik (site 10, Fig. 16b), the Huy2 envelope does not encompass the earliest two index points; although, as mentioned previously, these data are from an area some distance from the other lakes cored and so should perhaps be plotted on a separate graph (across the Nanortalik lake locations there is a c. 7 m spread in predicted RSL at 14 ka BP). Similar to the GREEN1 Greenland model of Fleming and Lambeck (2004), sea-level predictions for Huy2 suggest insufficient LGM ice load for southern Greenland. Huy2 has LGM (21 ka BP) ice thicknesses of c. 1100 m at Qaqortoq (site 9, Fig. 16b) and c. 900 m at Nanortalik (site 10). A synthesis of the available data by Weidick et al. (2004) suggests that the ice margin in south Greenland was behind its present-day position from c. 9 ka BP. The retreat of Huy2 is not continuous but roughly commences after 16 ka BP and, with good agreement to the observations, reaches the present-day modelled margin at c. 9 ka BP. Another GIA modelling study, in which the best-fit prediction shows good agreement with the RSL data, indicates the ice sheet started an earlier retreat from its LGM position at 22 ka BP and was inland of the present-day coast by 12 ka BP (Sparrenbom, Ph.D. thesis).

The preliminary findings of Long et al. (2008) indicate that the LGM ice load in southeast Greenland as represented in the Huy1 and GrB models is insufficient. The analyses here show that if we allow the GrIS to extend to the shelf edge with retreat off the shelf occurring c. 12 ka BP, the best-fit prediction for Ammassalik (site 11, Fig. 16b) reaches the HML, but does not give fit to the index point data. However, the rate of sea-level fall is reasonably well reproduced by Huy2 and the lower bound of the envelope indicates a fit to the observations may be achieved.

In a similar manner, the lower bound of the predicted RSL envelope tracks the data quite well for both Jameson Land (site 12, Fig. 16b) and Mesters Vig (site 13, Fig. 16b) in the east. Huy2 shows the fjord ice-free with ice having retreated to the present-day ice margin by 9 ka BP. A date of deglaciation c. 8–7.5 ka BP (Funder, 1987) close to the ice margin suggests a slightly later retreat.

In northeast Greenland, results from Kronprins Eijland (site 17, Fig. 16c), where upper limiting dates can further constrain the predictions, indicate a similar pattern of data-model misfit as seen from southeast and east Greenland. This suggests there may be a common reason why a fit cannot be achieved to RSL observations across the entire east coastline. Huy2 shows a retreat behind the present-day ice margin close to Hvalrosodden (site 14, Fig. 16b) and the lower bound of the envelope indicates that predictions could produce a fall below present-day sea-level.

In north Greenland the best-fit prediction of Huy2 does not fit the data at Jorgen Bronlund (site 18, Fig. 16c). Given that the timing of initial predicted sea-level fall is largely insensitive to Earth structure the trend of observations at Jorgen Bronlund suggests the data-model misfit cannot be resolved using the Huy2 ice history.

Washington Land is close to the Nares Strait which separates Greenland from the neighbouring Ellesmere Island ice sheet. It is well established that these two ice sheets were coalesced at LGM (England, 1999); the final deglaciation of the strait is dated to c. 10 ka BP (Zreda et al., 1999). This is fairly consistent with the timing of ice retreat in Huy2. A synthesis of dates indicates that deglaciation started at the entrances of the strait with the central parts becoming ice-free later (England, 1999). This finding is supported by observations of the HML which show a general pattern of decline from the centre to the entrances of the strait (Bennike, 2002). The ice margin of Huy2 is made to terminate at the axis of the straits, it does not coalesce with Innuitian ice and we do not see the pattern of retreat inferred from the HML data. The Huy2 best-fit model shows a relatively good fit to lower limiting data that define a sea-level fall, although the temporal coverage of these data is poor. The Huy2 model does not show a fall below present-day sea level for northwest Greenland. The nearby Humboldt Gletscher outlet glacier is thought to have readvanced (Bennike, 2002) so we might expect a late transgression.

When compared to RSL predictions based on Huy1, those generated from the Huy2 best-fit model generally show an improved data-model fit. The Huy2 model improves the fit to the earliest RSL data and in the majority of cases ascertains the HML (except in

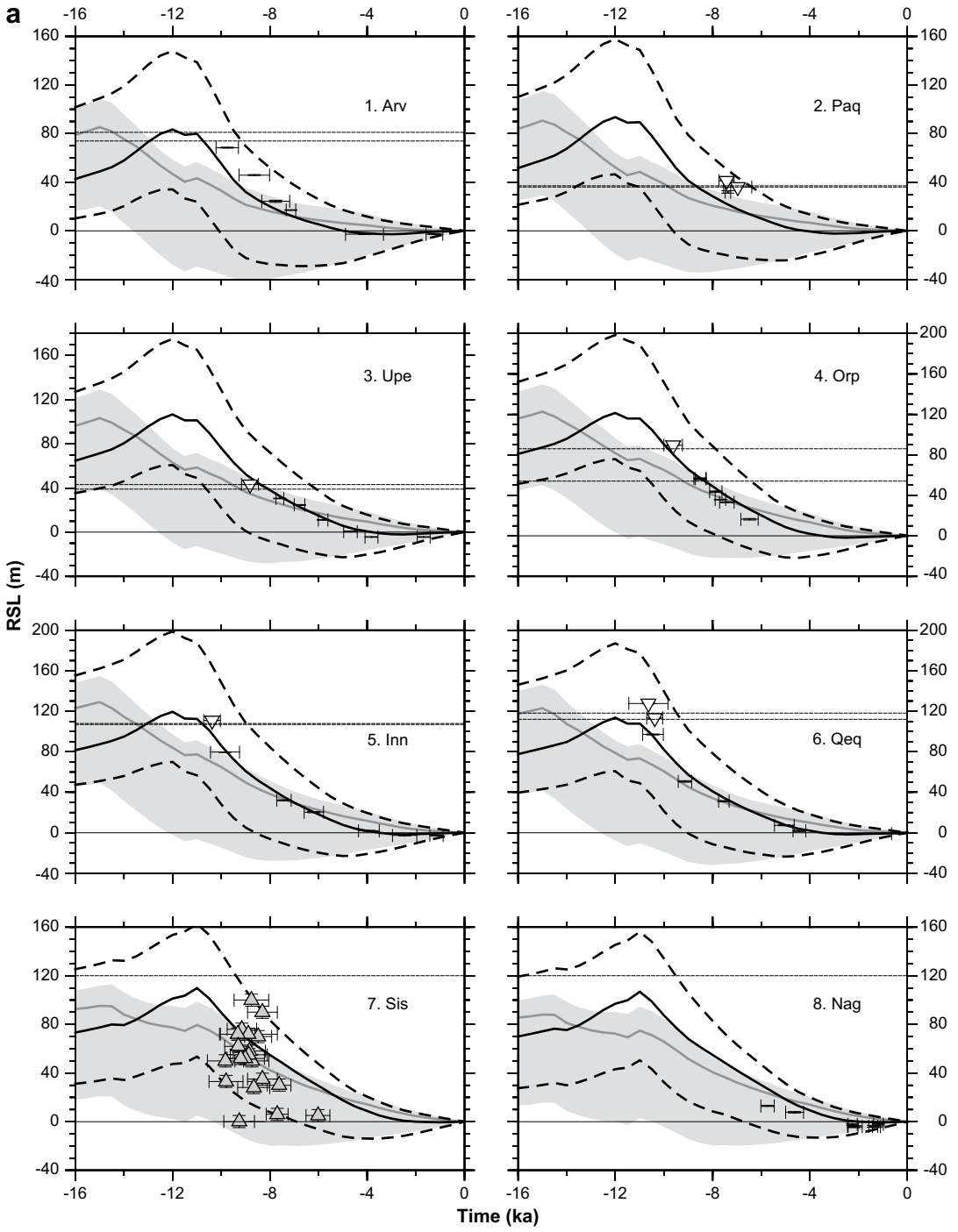

Fig. 16. RSL predictions for the Huy1 (light grey shaded area) and Huy2 (area enclosed by black dashed lines) ice models based on a suite of 108 Earth viscosity profiles. The solid dark grey line denotes the RSL prediction for the best-fit Earth model of Huy1; characterised by a 71 km thick lithosphere, upper mantle viscosity of 5×10^{20} Pa s and lower mantle viscosity of 5×10^{21} Pa s (see Sub-Section 3.1.2). The solid black line denotes the RSL prediction for the best-fit Earth model of Huy2; characterised by a 120 km thick lithosphere, upper mantle viscosity of 5×10^{20} Pa s and lower mantle viscosity of 10^{21} Pa s (see Sub-Section 3.3.1). The dotted black line shown for sites 11–17 indicates the Huy2 best-fit Earth model for regions across east Greenland; characterised by a 120 km thick lithosphere, upper mantle viscosity of 3×10^{20} Pa s and lower mantle viscosity of 5×10^{22} Pa s (see Sub-Section 4.2.3). Lower limiting dates are grey triangles. Upper limiting dates are inverted white triangles. Sea-level index points are represented by both time and height error bars. Qaqortoq (site 9) includes additional observational constraints, indicated by two extra horizontal dashed lines. The line at −8.7 m marks a marine basin that shows no evidence of freshwater incursion and defines a lower bound on RSL change. The line at 39.7 m and traced from 9.5 ka BP to present-day marks the minimum age of deglaciation for a basin and defines an upper bound on RSL change.

southwest and south Greenland). For Huy2, the timing of predicted initial RSL fall is later and therefore more rapid than Huy1 and shows better agreement with the data. In west Greenland where RSL observations record a fall below present-day sea level, the Huy2 prediction is able to reproduce this result well.

4. Discussion

The Huy2 model was calibrated using RSL data and observations of ice extent. In performing this calibration, we targeted ice model parameters that: (i) were effective in addressing large data-model

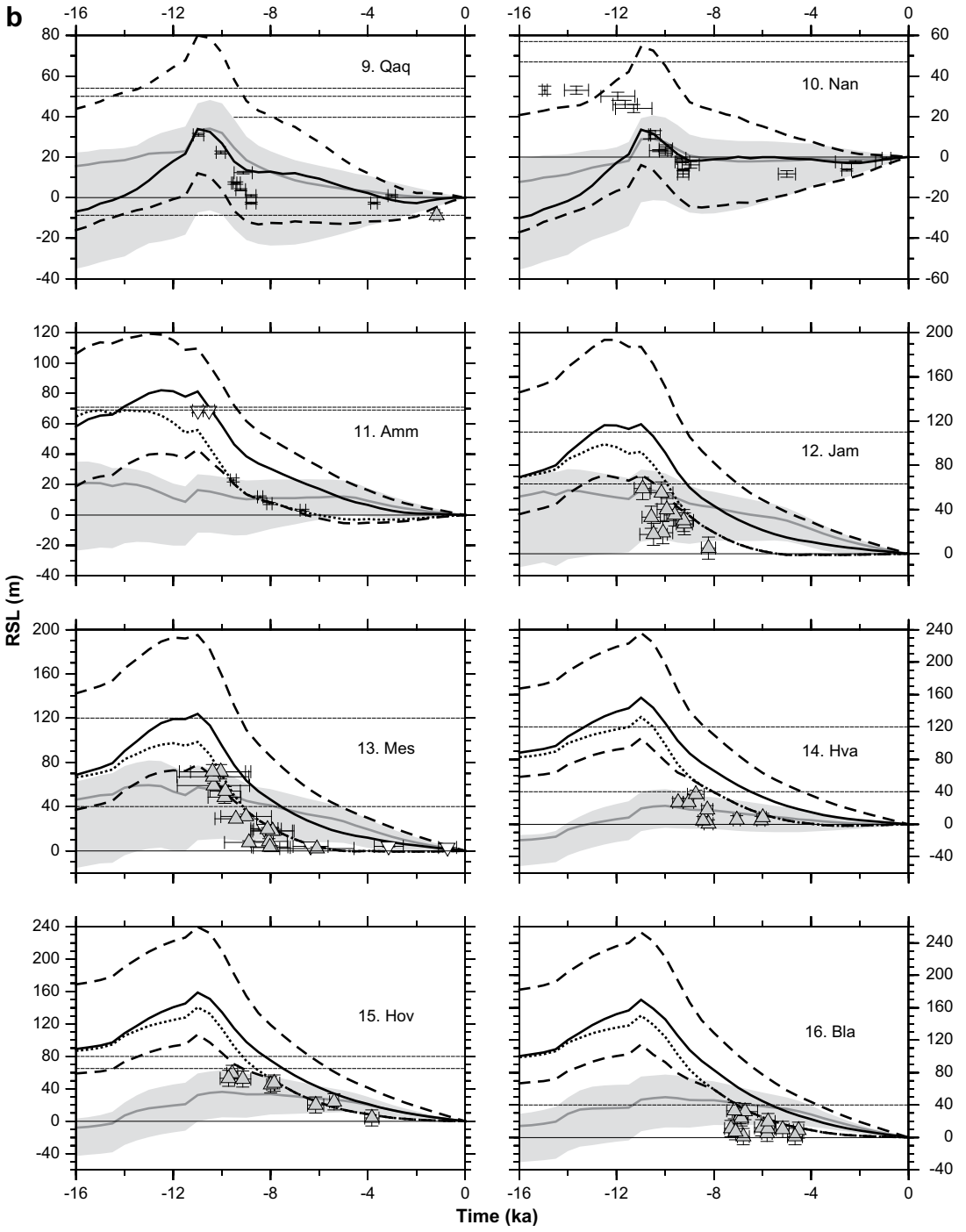

Fig. 16. (*continued*).

misfits and (ii) required revision from the previous Huy1 model based on recent observational constraints (LGM margin position, Holocene temperature forcing). Clearly, there are many other parameters that can be varied in our adopted ice model and so the solution (Huy2) is non-unique. However, a more complete sensitivity test goes beyond our aims in this study and so we refer the reader to past analyses of the GrIS for more detail in this regard (e.g. Calov and Hutter, 1996; Greve, 1997; Huybrechts, 1994, 1996, 2002; Ritz et al., 1997; Van de Wal, 1999). In addition, we note Zweck and Huybrechts (2005) performed a comprehensive sensitivity study of northern hemisphere ice sheet evolution in which 11 important parameters were varied. They found that climate parameters are the most important control on ice sheet evolution and extent, suggesting it is uncertainties in the climate forcing, rather than in the ice-dynamic model, that will introduce the largest errors. Changes to the parameters affecting ice flow have the largest influence on ice thickness and the profile of the ice sheet (see also Ritz et al., 1997). Parameter variations in the treatment of isostasy, marine calving and basal processes impacted ice evolution to a lesser degree. Making changes to some of these parameters, therefore, could lead to an alternative solution that provides an improved fit to the data.

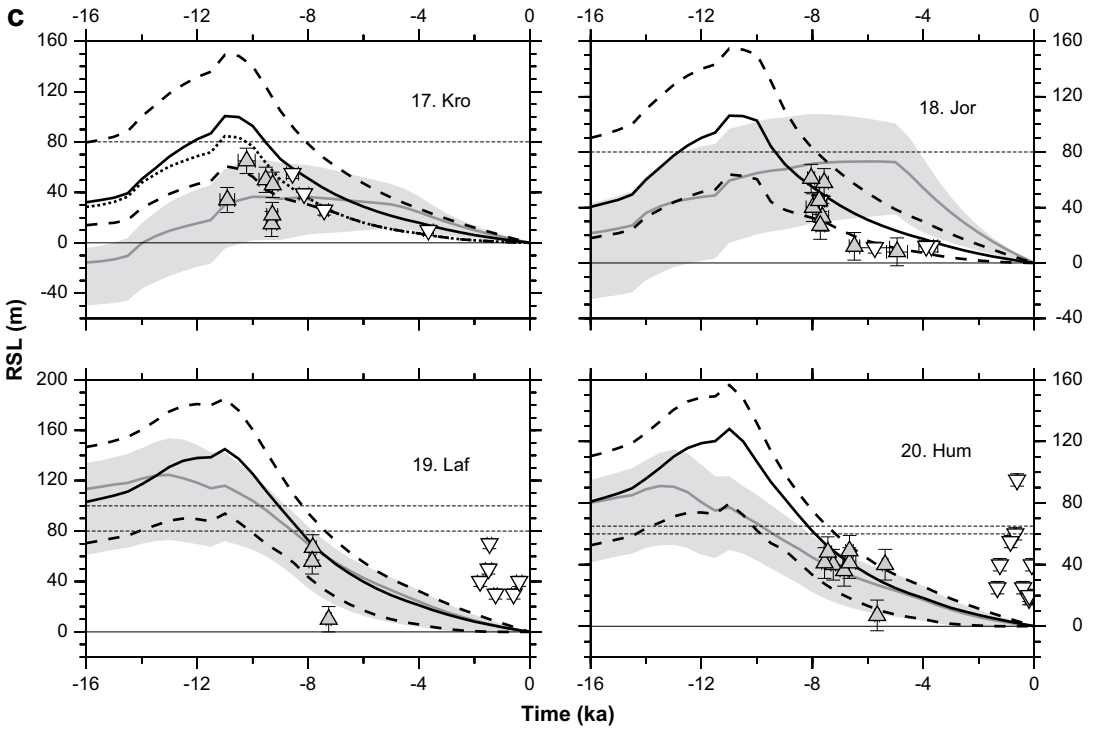

Fig. 16. (*continued*).

It is also plausible that some of the data-model misfits are due to limitations in our adopted ice and Earth models. With regard to the Earth model, the assumption of a laterally homogeneous Earth is likely one of the more significant (see Sub-Section 4.2.3). As outlined in the description of the ice model (see Sub-Sections 2.2 and 3.2), physical processes such as calving and ice stream dynamics are either poorly represented or absent, partly because some of these processes are not fully understood. The Huybrechts (2002) model is built upon the shallow ice approximation, as are the majority of current ice sheet models. Numerous studies have applied this approximation to successfully simulate the long-term behaviour of continental ice sheets like the GrIS (e.g. Greve, 1997; Huybrechts, 1996, 2002; Letréguilly et al., 1991; Ritz et al., 1997; Van de Wal, 1999). Although this approach can satisfactorily simulate large-scale dynamics, the approximation is inaccurate at the ice margin (Baral et al., 2001) and so could significantly impact our RSL predictions as these are sensitive to relatively small changes in margin position (see also Sub-Section 4.2.2). This issue is therefore an important target for future research. We note that there are a few three-dimensional ice sheet models which include higher-order stress gradients (e.g. Pattyn, 2003; Saito et al., 2003) but these are computationally intensive and so cannot be used effectively in the type of analysis presented here (which requires the generation of multiple simulations over 100 ka time intervals).

4.1. GrIS ice history and palaeoclimate: Huy2 model

4.1.1. Large-scale changes since the LGM

Broadly speaking the Huy2 model indicates a larger LGM extent and volume, a more rapid retreat from the continental shelf and larger retreat in response to the HTM when compared to the Huy1 model (Fig. 13). Ice thickness evolution for the times 18, 10 and 4 ka BP illustrates the major changes of the Huy2 model (Fig. 17). Accompanying plots of RSL evolution show that the 10 ka BP time-slice gives a close match to maps of the HML (Funder and Hansen, 1996; Weidick and Bennike, 2007). Huy2 has an LGM (21 ka BP) volume of 4.1 m (Huy1 has 2.7 m) excess ice-equivalent sea level; larger than the estimates of between 2 and 3 m from Clark and Mix (2002). Huybrechts (2002) finds, by altering crucial ice model parameters, LGM ice-equivalent sea level for Huy1 varied between 1.9 and 3.5 m (that is ±30% of his best estimate of 2.7 m). We would expect a similar ±30% variation in LGM ice-equivalent sea level for Huy2 if these sensitivity experiments were performed again. As with Huy1, the Huy2 model reaches its maximum volume at 16.5 ka BP, when it contains 4.6 m excess ice-equivalent sea level (Huy1 has 3.1 m). The volume is predicted to be a maximum at this time as increased accumulation rates in Greenland (Cuffey and Clow, 1997) still outweigh the larger ablation from increased temperatures. The sea-level forcing of Huy2 means the marine retreat does not begin in earnest until after 12 ka BP; changes to the ice sheet before this time are therefore driven, mainly, by temperature and accumulation changes. For comparison, the GrB model maintains its full glacial extent until 12 ka BP and reaches its maximum volume just prior to the Holocene, while GREEN1 favours a deglaciation starting at 14 ^{14}C (c. 16.3 ka BP). The subsequent marine retreat of Huy2 is very rapid and largely a consequence of the sea-level forcing. However, there is a difference between the maximum extent allowed by the marine parameterisation and the output from the model (Fig. 13), indicating that some aspects of the retreat were caused by increased temperatures. Warming that took place after the YD was abrupt and temperatures may have increased by 10 ± 4 °C in central Greenland (Grachev and Severinghaus, 2005).

4.1.2. The retreat behind present-day ice margin and neoglacial regrowth

For Huy2, the timing of retreat behind the present-day modelled margin is between 8 and 6 ka BP in west and southwest Greenland and around 9 ka BP in the south (Fig. 11). This is in good agreement with both the regional observations described above and a synthesis of deglaciation dates taken from close to the present-day ice margin

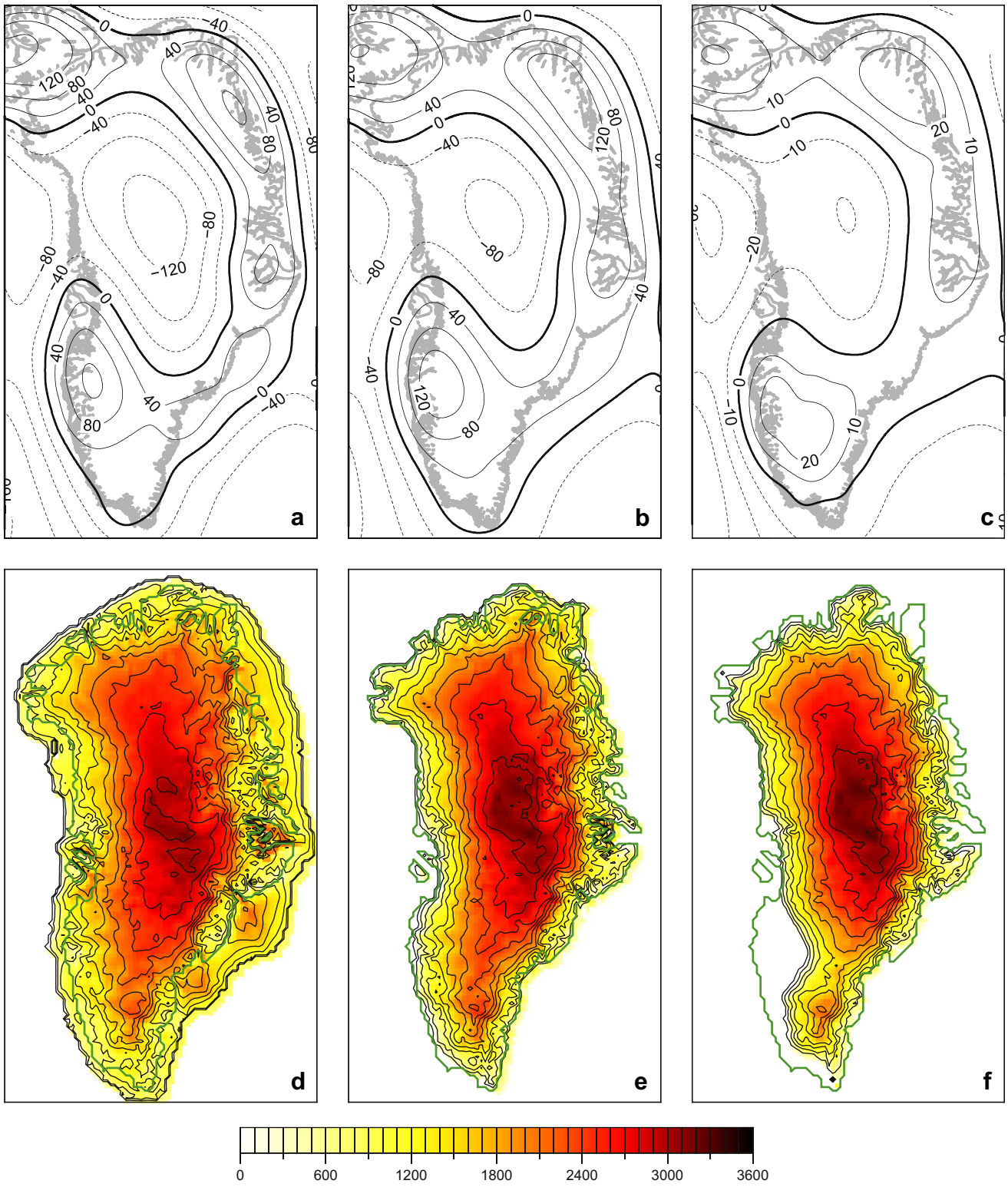

Fig. 17. Top frames show spatial plots of RSL (metres) generated from Huy2 with our reference Earth model for the times (a) 18, (b) 10 and (c) 4 ka BP. Actual coastline is outlined by the grey line. Bottom frames show Huy2 ice thickness evolution (in metres) for the times (d) 18, (e) 10 and (f) 4 ka BP. Modelled present-day coastline is outlined by the green line.

(Bennike, 2008). Huy2 reaches a minimum state at 4–5 ka BP with a retreat of up to 80 km in the southwest, 20 km in the south and 80 km near Hvalrosodden (site 14) in the northeast of Greenland. We note that the horizontal resolution of the model (20 km) limits the accuracy and reliability of margin prediction over these relatively short distances. The response to the HTM corresponds to a deficit volume of 0.17 m ice-equivalent sea level (relative to present-day); illustrating that changes in the ice margin position, of the order of 10s km, correspond to small changes in eustatic sea-level. In comparison, Huy1 predicts a minimum state at 3 ka BP with

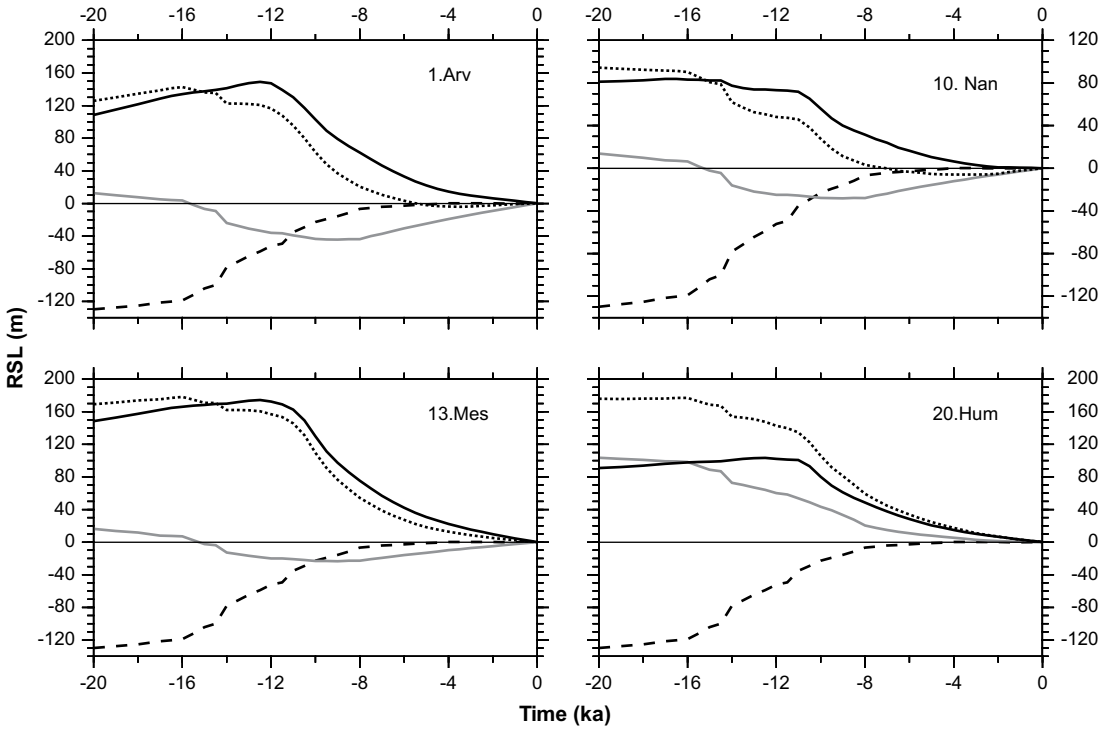

Fig. 18. The influence of Greenland ice load (Huy2; solid black), non-Greenland ice load (ICE-5G; grey line) and their sum (black dotted) on sea-level predictions at four sites around Greenland for our reference Earth model. The black dashed line represents eustatic sea level for the total (Greenland plus non-Greenland) ice model.

a 50 km retreat in southwest Greenland but with very little change in ice volume. Some observational evidence at the ice front has enabled the reconstruction of past glacial transport routes that suggest the ice margin in west Greenland was 15–20 km inland of its current position (Weidick et al., 1990). Previous ice modelling studies that compared model output with dated recessional moraine systems (Van Tatenhove et al., 1995, 1996) place the retreat up to 50 km behind the present-day modelled margin in southwest Greenland. Fleming and Lambeck (2004) introduce a neoglacial component to GREEN1 which suggests a retreat of c. 40 km behind the observed present-day margin in west Greenland. Tarasov and Peltier (2002) show ice volume and margin changes for GrB that

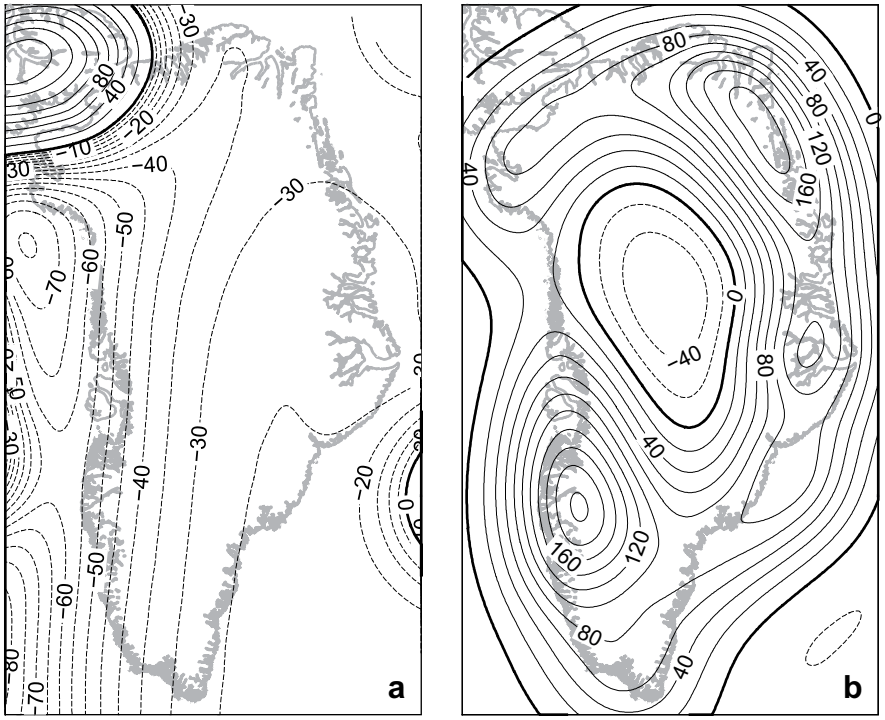

Fig. 19. Spatial plots of RSL predictions (in metres) generated using our reference Earth model and showing the vertical land motion component at 10 ka BP; for (a) non-Greenland ice (ICE-5G) and (b) Greenland ice (Huy2).

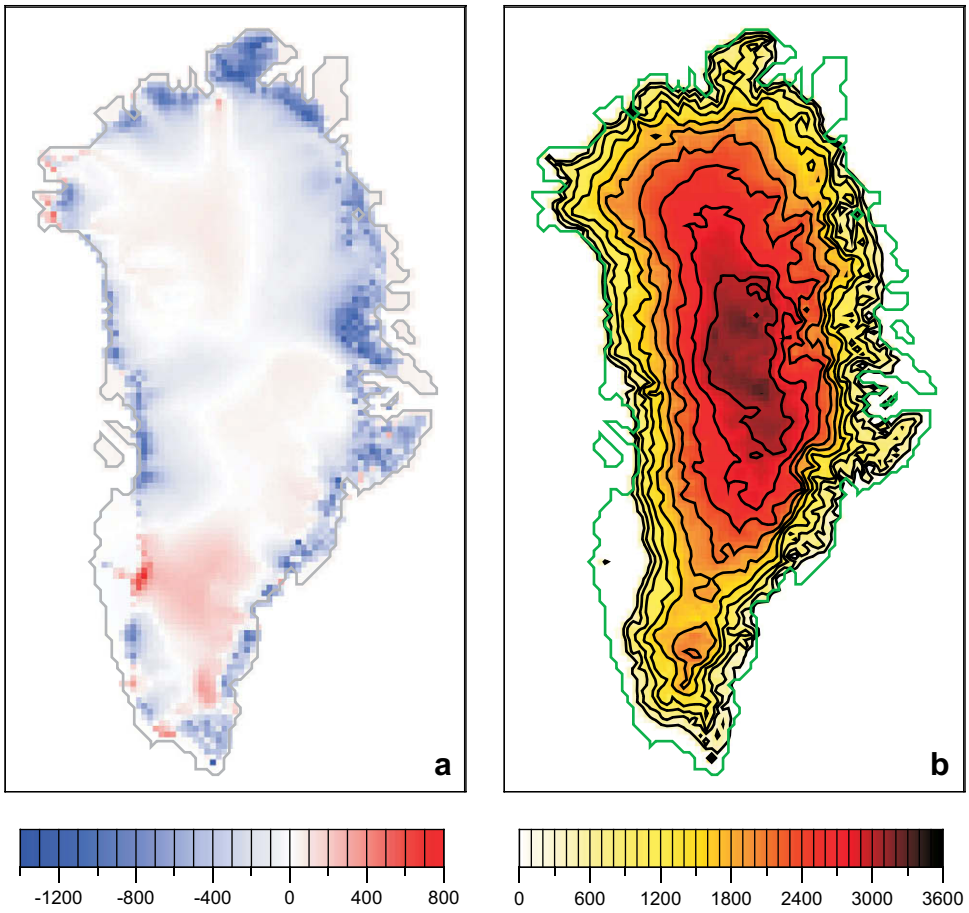

Fig. 20. (a) Observed minus modelled (Huy2) ice surface elevation (metres). Modelled present-day coastline is outlined in dark grey. (b) Huy2 modelled present-day ice thickness (metres). Modelled present-day coastline is outlined in green.

indicate the ice model reached a minimum state around 8 ka BP (the magnitude of margin retreat was not specified). These latter two studies concluded that a neoglacial regrowth of the GrIS is required to fit RSL data from west Greenland. We note that Sparrenbom (Ph.D. thesis) reached the same conclusion for the south of Greenland.

4.2. Data-model misfits

The results shown in Fig. 16 show that the Huy2 ice model cannot account for all data-model misfits evident from Huy1 in Fig. 5 (for a wide range of plausible 1-D viscosity models). Here we briefly consider the influence of non-Greenland ice load, the mismatch between present-day observed and modelled ice surface elevation and lateral changes in Earth structure.

4.2.1. Role of non-Greenland ice load

The total global ice load, as outlined previously, is the amalgamation of Greenland ice (Huy1 or Huy2) and non-Greenland ice (ICE-5G). Given the close proximity of some ice sheets to Greenland, most prominently the late Laurentide ice sheet, it is not surprising that they have an effect on the sea-level history of Greenland. Fleming and Lambeck (2004) demonstrated that together the North American and European ice sheets made a contribution to sea-level change around Greenland on the order of 10s of metres. It should be noted that in the ICE-5G reconstruction, North American ice load has an LGM volume of 74 m ice-equivalent sea level and is characterised by a multidomal structure (see Peltier (2002) for the model description). The influence of the ICE-5G loading history, minus the Greenland component, on RSL predictions is shown in Fig. 18. For Arveprinsen (site 1), Nanortalik (site 10) and Mesters Vig (site 13), we find that non-Greenland ice mass loss and the associated direct effect dominate the predictions at early times and this results in RSL fall. After 8 ka BP, North American ice has largely melted and so the dominant effect is vertical land motion associated with subsidence of the peripheral bulge leading to a net RSL rise. This pattern of RSL change is broadly similar to the results of Fleming and Lambeck (2004); although we note that there are significant differences in northwest Greenland. At Humboldt Gletscher (site 20, Fig. 18), for example, we find predictions show a continuous fall from c. 150 m at 20 ka BP. Lafayette Bugt is in such close proximity to Ellesmere ice that the solid surface undergoes postglacial rebound rather than forebulge collapse.

Over the Holocene period we find that RSL change driven by non-Greenland ice load changes can sometimes be equal and opposite to that driven by Greenland ice load changes. This effect is particularly marked for sites in the west and south. At Nanortalik (site 10, Fig. 18), for example, at 8 ka BP the predictions for non-Greenland and Greenland ice load are −30 and 30 m, respectively. Two spatial plots show the influence of vertical land motion on RSL from Greenland and non-Greenland ice at 10 ka BP (Fig. 19).

4.2.2. Comparison to present-day ice sheet

Huy2 gives a root mean square fit to the observed surface elevation and ice thickness of 292.1 and 239.3 m, respectively (the Huy1 model gives very similar values of 293 and 238.7 m).

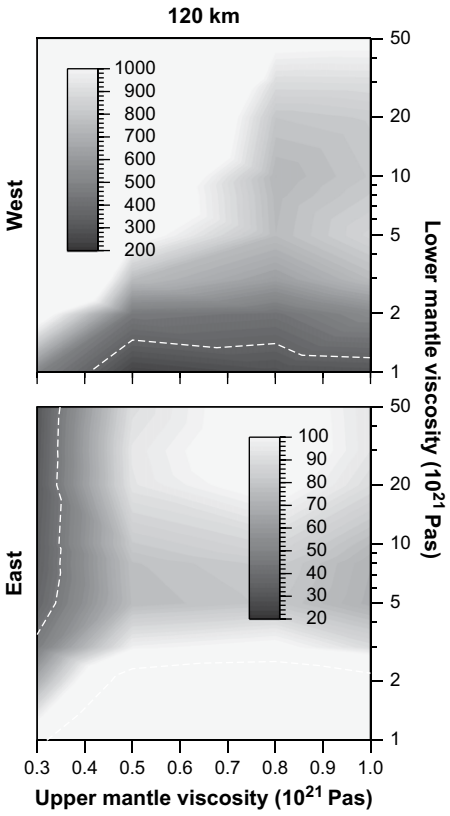

Fig. 21. The Chi-squared test based on the Huy2 ice model and assuming a 120 km thick lithosphere. The two frames are based on data from either west (top) or east (bottom) Greenland. A scale bar for the Chi-squared results is shown how in each frame (note the difference in magnitude between frames). The 95% confidence level is marked by the white dashed line.

Observations of present-day ice sheet elevation and thickness have been adapted (P. Huybrechts, personal communication) from Bamber et al. (2001). The difference between observed and modelled (Huy2) ice surface elevation (Fig. 20) is small over the central parts of the ice sheet and large at the ice margin. The model clearly over-predicts present-day ice elevation (and thickness although not shown) along the margin. This misfit appears largely due to differences between the location of the modelled and observed ice margin. The gradient at the margin is steep and a misfit between observed and modelled ice margin location will result in large differences between the corresponding observed and modelled ice elevation. This will have repercussions for the predicted RSL histories since they are very sensitive to changes in the ice margin position. The misfits between observations and model are a combination of the simplifications made in the climatic forcing, the physics of ice flow (see start of Section 4), and shortcomings in the observational data used as input. It is difficult to ascertain exactly which factors are dominant and therefore explain certain features in Fig. 20a. Another likely reason for the misfit is the ice model grid spacing, which is too large to resolve or account for small-scale processes at the margin. The 20 km ice model discretisation, which is standard in many glacial cycle simulations, is now regarded as too course. Moreover, conventional numerical schemes are known to introduce systematic errors at the ice margin (Huybrechts et al., 1996; Van den Berg et al., 2006).

4.2.3. Lateral changes in Earth structure

The Earth models used in this and the majority of GIA studies are 1-D only and so do not account for lateral variations in Earth structure. This model limitation may offer another explanation as to why data-model misfits cannot be reconciled. The geology of Greenland is largely Precambrian in age with flood basalts present on the central west and east coastline that define the past track of the Iceland plume beneath the continent (Henriksen et al., 2000; Storey et al., 2004). The trace of the plume track may indicate why there is a general trend of decreasing seismological lithospheric thickness as you move from west to east (Kumar et al., 2005). Farther east in Iceland, rapid rates of postglacial rebound indicate a very thin mechanical thickness (Sigmundsson, 1991). Darbyshire et al. (2004) find a similar pattern of decreasing seismological lithospheric thickness; they also find that the lithosphere exhibits higher shear wave velocities than the seismic model PREM (on which our Earth model is based) (Dziewonski and Anderson, 1981).

In order to make a preliminary assessment of the magnitude of lateral structure required to address some of the remaining data-model misfits, we divide the RSL data between west Greenland (sites 1–8) and regions across east Greenland (sites 11–17). Data outside these regions are omitted. For these separate datasets the χ^2 test is repeated and, in this case, the observational error of the limiting dates is taken into account. For the case of a 120 km thick lithosphere, the east Greenland data very clearly favour a reduced upper mantle viscosity when compared to west Greenland (Fig. 21). A plot of the east Greenland best-fit model (Fig. 16, dotted black line) illustrates the excellent fit that can be achieved when fitting these data independently. This result certainly suggests that lateral variation in Earth properties can accommodate at least some of the data-model misfit shown in Fig. 16.

5. Conclusions

1. The new Huy2 ice history for Greenland shows good agreement to the sea-level data and is also well constrained by independent observations of ice extent.
2. The Huy2 model contains 4.1 m excess ice-equivalent sea level at the LGM (21 ka BP); this is larger than previously found, mainly because the ice sheet now grounds further out on the continental shelf in the east. The ice sheet did not reach its maximum volume of 4.6 m excess ice-equivalent sea level until 16.5 ka BP.
3. Our results suggest that the ice margin retreat from the continental shelf may not have been continuous and a readvance may have occurred over the Younger Dryas period. Final retreat from the continental shelf began late (c. 12 ka BP) and retreat was rapid such that the GrIS was inland of the present-day coastline by 10 ka BP.
4. The reaction of the ice sheet to the Holocene Thermal Maximum may have produced a margin retreat of up to 80 km across the southwest sector of the ice sheet. This corresponds to a deficit volume of 0.17 m ice-equivalent sea level. This relatively large response of the GrIS to the imposed HTM improves the RSL data-model fit but we cannot be sure that it is a robust constraint given uncertainties in other model parameters.
5. The role of non-Greenland ice is significant. Especially over the last 8 ka BP across the southwest sector where Greenland and non-Greenland contributions to RSL are equal and opposite.
6. The fit of Huy2 (and Huy1) to present-day observations indicates that the model does not accurately reproduce the present ice terminus position and over-predicts ice load at the margin. This will likely have a significant impact on the RSL predictions.
7. A significant improvement to the RSL data-model fit was obtained when modelling data from the east and west independently. This suggests an east–west change in Earth structure. On the other hand, it is also plausible that these differences reflect inaccuracies in the modelled pattern of ice margin retreat (see Sub-Section 3.2.2).

Acknowledgements

This work was funded by the Natural Environment Research Council of the UK (project NE/C519311/1). We thank Kevin Fleming and two anonymous referees for useful and constructive comments on the original manuscript. We are grateful to Ole Bennike for providing a compilation of sea-level data from Sisimiut. This paper is a contribution to International Geological Correlation Programme Project 495 "Quaternary Land-Ocean Interactions" and the International Quaternary Association working group on "Coastal and Marine Processes". Most of the figures were produced using the GMT graphics software.

References

Andrews, J.T., 2008. The role of the Iceland ice sheet in the north Atlantic during the late Quaternary: a review and evidence from Denmark Strait. Journal of Quaternary Science 23 (1), 3–20.

Bamber, J.L., Layberry, R.L., Gogineni, S., 2001. A new ice thickness and bed data set for the Greenland ice sheet 1. Measurement, data reduction, and errors. Journal of Geophysical Research – Atmospheres 106 (D24), 33773–33780.

Baral, D.R., Hutter, K., Greve, R., 2001. Asymptotic theories of large-scale motion, temperature, and moisture distribution in land-based polythermal ice sheets: a critical review and new developments. Applied Mechanics Reviews 54 (3), 215–256.

Bennike, O., 1995. Paleoecology of 2 lake basins from Disko, west Greenland. Journal of Quaternary Science 10 (2), 149–155.

Bennike, O., 2002. Late Quaternary history of Washington Land, north Greenland. Boreas 31 (3), 260–272.

Bennike, O., 2008. An early Holocene Greenland whale from Melville Bugt, Greenland. Quaternary Research 69 (1), 72–76.

Bennike, O., Björck, S., 2002. Chronology of the last recession of the Greenland ice sheet. Journal of Quaternary Science 17 (3), 211–219.

Bennike, O., Björck, S., Lambeck, K., 2002. Estimates of south Greenland late-glacial ice limits from a new relative sea level curve. Earth and Planetary Science Letters 197 (3–4), 171–186.

Bennike, O., Hansen, K.B., Knudsen, K.L., Penney, D.N., Rasmussen, K.L., 1994. Quaternary marine stratigraphy and geochronology in central west Greenland. Boreas 23 (2), 194–215.

Bennike, O., Weidick, A., 2001. Late Quaternary history around Nioghalvfjerdsfjorden and Jokelbugten, north-east Greenland. Boreas 30 (3), 205–227.

Bentley, M.J., Fogwill, C.J., Kubik, P.W., Sugden, D.E., 2006. Geomorphological evidence and cosmogenic Be-10/Al-26 exposure ages for the Last Glacial Maximum and deglaciation of the Antarctic Peninsula ice sheet. Geological Society of America Bulletin 118 (9–10), 1149–1159.

Bindschadler, R.A., 1984. Jakobshavn Glacier Drainage-Basin – a balance assessment. Journal of Geophysical Research – Oceans 89 (NC2), 2066–2072.

Braithwaite, R.J., 1995. Positive degree-day factors for ablation on the Greenland ice-sheet studied by energy-balance modeling. Journal of Glaciology 41 (137), 153–160.

Brett, C.P., Zarudzki, E.F.K., 1979. Project Westmar, a shallow marine geophysical survey on the west Greenland shelf. Rapport Grønlands Geologiske Undersøgelse 87, 27.

Calov, R., Hutter, K., 1996. The thermomechanical response of the Greenland ice sheet to various climate scenarios. Climate Dynamics 12, 243–260.

Clark, P.U., Mix, A.C., 2002. Ice sheets and sea level of the Last Glacial Maximum. Quaternary Science Reviews 21 (1–3), 1–7.

Cuffey, K.M., 2000. Methodology for use of isotopic climate forcings in ice sheet models. Geophysical Research Letters 27 (19), 3065–3068.

Cuffey, K.M., Clow, G.D., 1997. Temperature, accumulation, and ice sheet elevation in central Greenland through the last deglacial transition. Journal of Geophysical Research – Oceans 102 (C12), 26383–26396.

Cuffey, K.M., Clow, G.D., Alley, R.B., Stuiver, M., Waddington, E.D., Saltus, R.W., 1995. Large arctic temperature-change at the Wisconsin-Holocene glacial transition. Science 270 (5235), 455–458.

Dahl Jensen, D., Mosegaard, K., Gundestrup, N., Clow, G.D., Johnsen, S.J., Hansen, A.W., Balling, N., 1998. Past temperatures directly from the Greenland ice sheet. Science 282 (5387), 268–271.

Dansgaard, W., Johnsen, S.J., Clausen, H.B., Dahl Jensen, D., Gundestrup, N.S., Hammer, C.U., Hvidberg, C.S., Steffensen, J.P., Sveinbjornsdottir, A.E., Jouzel, J., Bond, G., 1993. Evidence for general instability of past climate from a 250-Kyr ice-core record. Nature 364 (6434), 218–220.

Dansgaard, W., Johnsen, S.J., Clausen, H.B., Langway Jr., C.C., 1971. Climatic record revealed by the Camp Century ice core. In: Turekian, K.K. (Ed.), The Late Cenozoic Glacial Ages. Yale University Press, New Haven, CT, pp. 37–56.

Darbyshire, F.A., Larsen, T.B., Mosegaard, K., Dahl-Jensen, T., Gudmundsson, Ó., Bach, T., Gregersen, S., Pedersen, H.A., Hanka, W., 2004. A first detailed look at the Greenland lithosphere and upper mantle, using Rayleigh wave tomography. Geophysical Journal International 158 (1), 267–286.

Denton, G., Hughes, T., 1981. The Last Great Ice Sheets. Wiley, New York.

Dowdeswell, J.A., Whittington, R.J., Marienfeld, P., 1994. The origin of massive diamicton facies by iceberg rafting and scouring, Scoresby-Sund, east Greenland. Sedimentology 41 (1), 21–35.

Dyke, A.S., Prest, V.K., 1987. Late Wisconsinan and Holocene Retreat of the Laurentide Ice Sheet. Scale 1:5,000,000. Map 1702A. In: Geological Survey of Canada, Ottawa, Ontario, Canada.

Dziewonski, A.M., Anderson, D.L., 1981. Preliminary reference Earth model. Physics of the Earth and Planetary Interiors 25 (4), 297–356.

Ekholm, S., 1996. A full coverage, high-resolution, topographic model of Greenland computed from a variety of digital elevation data. Journal of Geophysical Research – Solid Earth 101 (B10), 21961–21972.

England, J., 1999. Coalescent Greenland and Innuitian ice during the Last Glacial Maximum: revising the Quaternary of the Canadian High Arctic. Quaternary Science Reviews 18 (3), 421–456.

Evans, J., Dowdeswell, J.A., Grobe, H., Niessen, F., Stein, R., Hubberten, H.W., Whittington, R.J., 2002. Late Quaternary sedimentation in Kejser Franz Joseph Fjord and the continental margin of east Greenland. In: Dowdeswell, J.A., O'Cofaigh, C. (Eds.), Glacier-Influenced Sedimentation on High-Latitude Continental Margins. Geological Society of London, London, United Kingdom.

Fairbanks, R.G., 1989. A 17,000-year glacio-eustatic sea-level record – influence of glacial melting rates on the Younger Dryas event and deep-ocean circulation. Nature 342 (6250), 637–642.

Farrell, W.E., Clark, J.A., 1976. Postglacial sea-level. Geophysical Journal of the Royal Astronomical Society 46 (3), 647–667.

Fleming, K., Lambeck, K., 2004. Constraints on the Greenland ice sheet since the Last Glacial Maximum from sea-level observations and glacial-rebound models. Quaternary Science Reviews 23 (9–10), 1053–1077.

Funder, S., 1987. Quaternary Geology and Landforms of the Coast of Jameson Land, East Greenland. In: Geological Survey of Greenland, Copenhagen (map sheet).

Funder, S., Abrahamsen, N., 1988. Palynology in a polar desert, eastern north Greenland. Boreas 17 (2), 195–207.

Funder, S., 1989. Quaternary geology of the ice-free areas and adjacent shelves of Greenland. In: Fulton, R.J. (Ed.), Quaternary Geology of Canada and Greenland. Geological Survey of Canada, pp. 741–792.

Funder, S., Hansen, L., 1996. The Greenland ice sheet – a model for its culmination and decay during and after the Last Glacial Maximum. Bulletin of the Geological Society of Denmark 42, 137–152.

Funder, S., Hjort, C., Landvik, J.Y., Nam, S.I., Reeh, N., Stein, R., 1998. History of a stable ice margin east Greenland during the Middle and Upper Pleistocene. Quaternary Science Reviews 17 (1–3), 77–123.

Gotfredsen, A.B., Møberg, T., 2004. Nipisat – a Saqqaq culture site in Sisimiut, central west Greenland. Meddelelser om Grønland, Man and Society 31.

Grachev, A.M., Severinghaus, J.P., 2005. A revised $+10 \pm 4$ degrees C magnitude of the abrupt change in Greenland temperature at the Younger Dryas termination using published GISP2 gas isotope data and air thermal diffusion constants. Quaternary Science Reviews 24 (5–6), 513–519.

Greve, R., 1997. Application of a polythermal three-dimensional ice sheet model to the Greenland ice sheet: response to steady-state and transient climate scenarios. Journal of Climate 10 (5), 901–918.

Håkansson, L., Briner, J., Alexanderson, H., Aldahan, A., Possnert, G., 2007. Be-10 ages from central east Greenland constrain the extent of the Greenland ice sheet during the Last Glacial Maximum. Quaternary Science Reviews 26 (19–21), 2316–2321.

Henriksen, N., Higgins, A.K., Kalsbeek, F., Pulvertaft, T.C.R., 2000. Greenland from Archaean to Quaternary. Geological Survey of Denmark and Greenland Bulletin 185.

Hjort, C., 1997. Glaciation, climate history, changing marine levels and the evolution of the northeast Water Polynya. Journal of Marine Systems 10 (1–4), 23–33.

Hutter, K., 1983. Theoretical Glaciology: Material Science of Ice and the Mechanics of Glaciers and Ice Sheets. Kluwer Academic, Norwell, Massachusetts.

Huybrechts, P., 1990. The Antarctic ice sheet during the last glacial–interglacial cycle: a three dimensional experiment. Annals of Glaciology 11, 52–59.

Huybrechts, P., 1994. The present evolution of the Greenland ice sheet: an assessment by modelling. Global and Planetary Change 9, 39–51.

Huybrechts, P., 1996. Basal temperature conditions of the Greenland ice sheet during the glacial cycles. Annals of Glaciology 23, 226–236.

Huybrechts, P., 2002. Sea-level changes at the LGM from ice-dynamic reconstructions of the Greenland and Antarctic ice sheets during the glacial cycles. Quaternary Science Reviews 21 (1–3), 203–231.

Huybrechts, P., de Wolde, J., 1999. The dynamic response of the Greenland and Antarctic ice sheets to multiple-century climatic warming. Journal of Climate 12 (8), 2169–2188.

Huybrechts, P., Payne, A.J., Abe-Ouchi, A., Calov, R., Fabre, A., Fastook, J.L., Greve, R., Hindmarsh, R.C.A., Høydal, O., Jóhannesson, T., MacAyeal, D.R., Marsiat, I., Ritz, C., Verbitsky, M.Y., Waddington, E.D., Warner, R., 1996. The EISMINT benchmarks for testing ice-sheet models. Annals of Glaciology 23, 1–12.

Ingolfsson, O., Frich, P., Funder, S., Humlum, O., 1990. Paleoclimatic implications of an early Holocene glacier advance on Disko-Island, west Greenland. Boreas 19 (4), 297–311.

Imbrie, J.Z., Hays, J.D., Martinson, D.G., MacIntyre, A., Mix, A.C., Morley, J.J., Pisias, N.G., Prell, W.L., Shackleton, N.J., 1984. The orbital theory of Pleistocene climate: support from a revised chronology of the marine d18O record. In: Berger, A., Imbrie, J.Z., Hays, J.D., Kukla, G., Saltzman, B. (Eds.). Milankovitch and Climate. D. Reidel, Dordrecht, pp. 269–305.

Janssens, I., Huybrechts, P., 2000. The treatment of meltwater retention in mass-balance parameterizations of the Greenland ice sheet. Annals of Glaciology 31, 133–140.
Jennings, A.E., Hald, M., Smith, M., Andrews, J.T., 2006. Freshwater forcing from the Greenland ice sheet during the Younger Dryas: evidence from southeastern Greenland shelf cores. Quaternary Science Reviews 25 (3–4), 282–298.
Jennings, A.E., Knudsen, K.L., Hald, M., Hansen, C.V., Andrews, J.T., 2002. A mid-Holocene shift in Arctic sea-ice variability on the east Greenland Shelf. Holocene 12 (1), 49–58.
Johnston, P., 1993. The effect of spatially nonuniform water loads on prediction of sea-level change. Geophysical Journal International 114 (3), 615–634.
Kaplan, M.R., Wolfe, A.P., Miller, G.H., 2002. Holocene environmental variability in southern Greenland inferred from lake sediments. Quaternary Research 58 (2), 149–159.
Kaufman, D.S., Ager, T.A., Anderson, N.J., Anderson, P.M., Andrews, J.T., Bartlein, P.J., Brubaker, L.B., Coats, L.L., Cwynar, L.C., Duvall, M.L., Dyke, A.S., Edwards, M.E., Eisner, W.R., Gajewski, K., Geirsdottir, A., Hu, F.S., Jennings, A.E., Kaplan, M.R., Kerwin, M.N., Lozhkin, A.V., MacDonald, G.M., Miller, G.H., Mock, C.J., Oswald, W.W., Otto-Bliesner, B.L., Porinchu, D.F., Ruhland, K., Smol, J.P., Steig, E.J., Wolfe, B.B., 2004. Holocene thermal maximum in the western Arctic (0–180 degrees W). Quaternary Science Reviews 23 (5–6), 529–560.
Kaufmann, G., Lambeck, K., 2000. Mantle dynamics, postglacial rebound and the radial viscosity profile. Physics of the Earth and Planetary Interiors 121 (3–4), 301–324.
Kaufmann, G., Lambeck, K., 2002. Glacial isostatic adjustment and the radial viscosity profile from inverse modeling. Journal of Geophysical Research – Solid Earth 107 (B11), 2280.
Kelly, M., 1979. Comments on the implications of new radiocarbon datings from the Holsteinsborg region, central west Greenland. Rapport Grønlands Geologiske Undersøgelse 95, 35–42.
Kelly, M., 1980. The status of the neoglacial in western Greenland. Rapport Grønlands Geologiske Undersøgelse 96, 24.
Kelly, M., 1985. A review of the Quaternary geology of western Greenland. In: Andrews, J.T. (Ed.), Quaternary Environments Eastern Canadian Arctic, Baffin Bay and Western Greenland. Allen and Unwin, Boston, pp. 461–501.
Kendall, R.A., Mitroviva, J.X., Milne, G.A., 2005. On post-glacial sea level: II. Numerical formulation and comparative results on spherically symmetric models. Geophysical Journal International 161 (3), 679–706.
Khan, S.A., Wahr, J., Leuliette, E., van Dam, T., Larson, K.M., Francis, O., 2008. Geodetic measurements of postglacial adjustments in Greenland. Journal of Geophysical Research – Solid Earth 113, B02402.
Koerner, R.M., Fisher, D.A., 1990. A record of Holocene summer climate from a Canadian High-Arctic Ice Core. Nature 343 (6259), 630–631.
Kuijpers, A., Troelstra, S.R., Prins, M.A., Linthout, K., Akhmetzhanov, A., Bouryak, S., Bachmann, M.F., Lassen, S., Rasmussen, S., Jensen, J.B., 2003. Late Quaternary sedimentary processes and ocean circulation changes at the southeast Greenland margin. Marine Geology 195 (1–4), 109–129.
Kumar, P., Kind, R., Hanka, W., Wylegalla, K., Reigber, C., Yuan, X., Woelbern, I., Schwintzer, P., Fleming, K., Dahl-Jensen, T., Larsen, T.B., Schweitzer, J., Priestley, K., Gudmundsson, O., Wolf, D., 2005. The lithosphere–asthenosphere boundary in the north-west Atlantic region. Earth and Planetary Science Letters 236 (1–2), 249–257.
Lambeck, K., Purcell, A., 2005. Sea-level change in the Mediterranean Sea since the LGM: model predictions for tectonically stable areas. Quaternary Science Reviews 24 (18–19), 1969–1988.
Lambeck, K., Smither, C., Johnston, P., 1998. Sea-level change, glacial rebound and mantle viscosity for northern Europe. Geophysical Journal International 134 (1), 102–144.
Landvik, J.Y., 1994. The last glaciation of Germania-land and adjacent areas, northeast Greenland. Journal of Quaternary Science 9 (1), 81–92.
Lemke, P., Ren, J., Alley, R.B., Allison, I., Carrasco, J., Flato, G., Fujii, Y., Kaser, G., Mote, P., Thomas, R.H., Zhang, T., 2007. Observations: changes in snow, ice and frozen ground. In: Solomon, S., Qin, D., Manning, M., Chen, Z., Marquis, M., Averyt, K.B., Tignor, M., Miller, H.L. (Eds.), Climate Change 2007: The Physical Science Basis. Contribution of Working Group 1 to the Fourth Assessment Report of the Intergovernmental Panel on Climate Change. Cambridge University Press, Cambridge, United Kingdom and New York, NY, USA.
Letréguilly, A., Reeh, N., Huybrechts, P., 1991. The Greenland ice-sheet through the Last Glacial interglacial cycle. Global and Planetary Change 90 (4), 385–394.
Lloyd, J.M., Park, L.A., Kuijpers, B., Moros, M., 2005. Early Holocene palaeoceanography and deglacial chronology of Disko Bugt, west Greenland. Quaternary Science Reviews 24 (14–15), 1741–1755.
Long, A., Woodroffe, S., Dawson, S., Roberts, D.H., Bryant, C., in press. Late Holocene relative sea level rise and the Neoglacial history of the Greenland ice sheet.
Long, A.J., Roberts, D.H., 2002. A revised chronology for the 'Fjord Stade' moraine in Disko Bugt, west Greenland. Journal of Quaternary Science 17 (5–6), 561–579.
Long, A.J., Roberts, D.H., 2003. Late Weichselian deglacial history of Disko Bugt, west Greenland, and the dynamics of the Jakobshavns Isbrae ice stream. Boreas 32 (1), 208–226.
Long, A.J., Roberts, D.H., Dawson, S., 2006. Early Holocene history of the west Greenland ice sheet and the GH-8.2 event. Quaternary Science Reviews 25 (9–10), 904–922.
Long, A.J., Roberts, D.H., Rasch, M., 2003. New observations on the relative sea level and deglacial history of Greenland from Innaarsuit, Disko Bug. Quaternary Research 60 (2), 162–171.
Long, A.J., Roberts, D.H., Simpson, M.J.R., Dawson, S., Milne, G.A., Huybrechts, P., 2008. Late Weichselian relative sea-level changes and ice sheet history in southeast Greenland. Earth and Planetary Science Letters 272 (1–2), 8–18.
Long, A.J., Roberts, D.H., Wright, M.R., 1999. Isolation basin stratigraphy and Holocene relative sea-level change on Arveprinsen Ejland, Disko Bugt, west Greenland. Journal of Quaternary Science 14 (4), 323–345.
Marshall, S.J., James, T.S., Clarke, G.K.C., 2002. North American ice sheet reconstructions at the Last Glacial Maximum. Quaternary Science Reviews 21 (1–3), 175–192.
Mienert, J., Andrews, J.T., Milliman, J.D., 1992. The east Greenland continental-margin (65-degrees-N) since the last deglaciation – changes in sea-floor properties and ocean circulation. Marine Geology 106 (3–4), 217–238.
Mikkelsen, N., Kuijpers, A., Arneborg, J., 2008. The Norse in Greenland and late Holocene sea-level change. Polar Record 44 (228), 45–50.
Milne, G.A., Mitrovica, J.X., 1996. Postglacial sea-level change on a rotating Earth: first results from a gravitationally self-consistent sea-level equation. Geophysical Journal International 126 (3), F13–F20.
Milne, G.A., Mitrovica, J.X., Davis, J.L., 1999. Near-field hydro-isostasy: the implementation of a revised sea-level equation. Geophysical Journal International 139 (2), 464–482.
Mitrovica, J.X., Forte, A.M., 1997. Radial profile of mantle viscosity: results from the joint inversion of convection and postglacial rebound observables. Journal of Geophysical Research – Solid Earth 102 (B2), 2751–2769.
Mitrovica, J.X., Forte, A.M., 2004. A new inference of mantle viscosity based upon joint inversion of convection and glacial isostatic adjustment data. Earth and Planetary Science Letters 225 (1–2), 177–189.
Mitrovica, J.X., Milne, G.A., 2003. On post-glacial sea level: I. General theory. Geophysical Journal International 154 (2), 253–267.
Mitrovica, J.X., Peltier, W.R., 1991. On postglacial geoid subsidence over the equatorial oceans. Journal of Geophysical Research – Solid Earth 96 (B12), 20053–20071.
Mitrovica, J.X., Peltier, W.R., 1993. The inference of mantle viscosity from an inversion of the Fennoscandian relaxation spectrum. Geophysical Journal International 114 (1), 45–62.
Mitrovica, J.X., Peltier, W.R., 1995. Constraints on mantle viscosity based upon the inversion of postglacial uplift data from the Hudson-Bay Region. Geophysical Journal International 122 (2), 353–377.
Nakada, M., Lambeck, K., 1987. Glacial rebound and relative sea-level variations – a new appraisal. Geophysical Journal of the Royal Astronomical Society 90 (1), 171–224.
Nam, S.I., Stein, R., Grobe, H., Hubberten, H., 1995. Late Quaternary glacial interglacial changes in sediment composition at the east Greenland continental-margin and their paleoceanographic implications. Marine Geology 122 (3), 243–262.
O'Cofaigh, C., Dowdeswell, J.A., Evans, J., Kenyon, N.H., Taylor, J., Mienert, A., Wilken, M., 2004. Timing and significance of glacially influenced mass-wasting in the submarine channels of the Greenland Basin. Marine Geology 207 (1–4), 39–54.
Pattyn, F., 2003. A new three-dimensional higher-order thermomechanical ice sheet model: basic sensitivity, ice stream development and ice flow across subglacial lakes. Journal of Geophysical Research – Solid Earth 108 (B8), 2382.
Peltier, W.R., 1974. The impulse response of a Maxwell Earth. Reviews of Geophysics and Space Physics 12, 649–669.
Peltier, W.R., 1994. Ice-age Paleotopography. Science 265 (5169), 195–201.
Peltier, W.R., 1996. Mantle viscosity and ice-age ice sheet topography. Science 273 (5280), 1359–1364.
Peltier, W.R., 2002. Global glacial isostatic adjustment: paleogeodetic and space-geodetic tests of the ICE-4G (VM2) model. Journal of Quaternary Science 17 (5–6), 491–510.
Peltier, W.R., 2004. Global glacial isostasy and the surface of the ice-age earth: the ICE-5G (VM2) model and grace. Annual Review of Earth and Planetary Sciences 32, 111–149.
Peltier, W.R., Jiang, X.H., 1996. Mantle viscosity from the simultaneous inversion of multiple data sets pertaining to postglacial rebound. Geophysical Research Letters 23 (5), 503–506.
Rasch, M., 2000. Holocene relative sea level changes in Disko Bugt, west Greenland. Journal of Coastal Research 16 (2), 306–315.
Rasch, M., Jensen, J.F., 1997. Ancient Eskimo dwelling sites and Holocene relative sealevel changes in southern Disko Bugt, central west Greenland. Polar Research 16 (2), 101–115.
Reimer, P.J., Baillie, M.G.L., Bard, E., Bayliss, A., Beck, J.W., Bertrand, C.J.H., Blackwell, P.G., Buck, C.E., Burr, G.S., Cutler, K.B., Damon, P.E., Edwards, R.L., Fairbanks, R.G., Friedrich, M., Guilderson, T.P., Hogg, A.G., Hughen, K.A., Kromer, B., McCormac, G., Manning, S., Ramsey, C.B., Reimer, R.W., Remmele, S., Southon, J.R., Stuiver, M., Talamo, S., Taylor, F.W., van der Plicht, J., Weyhenmeyer, C.E., 2004. IntCal04 terrestrial radiocarbon age calibration, 0–26 cal kyr BP. Radiocarbon 46 (3), 1029–1058.
Ritz, C., Fabre, A., Letréguilly, A., 1997. Sensitivity of a Greenland ice sheet model to ice flow and ablation parameters: consequences for the evolution through the last climatic cycle. Climate Dynamics 13, 11–24.
Roberts, D.H., Long, A.J., Schnabel, C., Freeman, S., Simpson, M.J.R., 2008. The deglacial history of southeast sector of the Greenland ice sheet during the Last Glacial Maximum. Quaternary Science Reviews 27 (15–16), 1505–1516.
Saito, F., Abe-Ouchi, A., Blatter, H., 2003. Effects of first-order stress gradients in an ice sheet evaluated by a three-dimensional thermomechanical coupled model. Annals of Glaciology 37, 166–172.
Schoof, C., 2007. Ice sheet grounding line dynamics: steady states, stability, and hysteresis. Journal of Geophysical Research – Earth Surface 112, F3.

Shennan, I., 1986. Flandrian sea-level changes in the Fenland. II: tendencies of sea-level movement, altitudinal changes, and local and regional factors. Journal of Quaternary Science 1 (2), 155–179.
Sigmundsson, F., 1991. Post-glacial rebound and asthenosphere viscosity in Iceland. Geophysical Research Letters 18 (6), 1131–1134.
Smith, L.M., Licht, K.J., 2000. Radiocarbon Date List IX: Antarctica, Arctic Ocean, and the Northern North Atlantic. Institute of Arctic and Alpine Research, Occasional Paper, 54, pp. 138.
Solheim, A., Faleide, J.I., Andersen, E.S., Elverhoi, A., Forsberg, C.F., Vanneste, K., Uenzelmann-Neben, G., Channell, J.E.T., 1998. Late Cenozoic seismic stratigraphy and glacial geological development of the east Greenland and Svalbard Barents Sea continental margins. Quaternary Science Reviews 17 (1–3), 155–184.
Sparrenbom, C.J., 2006. Constraining the Southern Part of the Greenland Ice Sheet since the Last Glacial Maximum from Relative Sea-Level Changes, Cosmogenic Dates and Glacial-Isostatic Adjustment Models. Ph.D. thesis. Centre for Geo-Biosphere Science, Lund University.
Sparrenbom, C.J., Bennike, O., Bjorck, S., Lambeck, K., 2006. Relative sea-level changes since 15 000 cal. yr BP in the Nanortalik area, southern Greenland. Journal of Quaternary Science 21 (1), 29–48.
Sparrenbom, C.J., Bennike, O., Bjorck, S., Lambeck, K., 2006. Holocene relative sea-level changes in the Qaqortoq area, southern Greenland. Boreas 35 (2), 171–187.
Storey, M., Pedersen, A.K., Stecher, O., Bernstein, S., Larsen, H.C., Larsen, L.M., Baker, J.A., Duncan, R.A., 2004. Long-lived postbreakup magmatism along the east Greenland margin: evidence for shallow-mantle metasomatism by the Iceland plume. Geology 32 (2), 173–176.
Stuiver, M., Reimer, P.J., 1993. Extended C-14 revised calib 3.0 C-14 age calibration program. Radiocarbon 35 (1), 215–230.
Tarasov, L., Peltier, W.R., 2002. Greenland glacial history and local geodynamic consequences. Geophysical Journal International 150 (1), 198–229.
Tarasov, L., Peltier, W.R., 2004. A geophysically constrained large ensemble analysis of the deglacial history of the North American ice-sheet complex. Quaternary Science Reviews 23 (3–4), 359–388.
Ten Brink, N.W., Weidick, A., 1974. Greenland ice sheet history since the last glaciation. Quaternary Research 4, 429–440.
Trautman, M.A., Willis, E.H., 1963. Isotopes, Inc., radiocarbon measurements III. Radiocarbon 5, 62–79.
Tushingham, A.M., Peltier, W.R., 1991. ICE-3G – a new global-model of late Pleistocene deglaciation based upon geophysical predictions of postglacial relative sea-level change. Journal of Geophysical Research – Solid Earth and Planets 96 (B3), 4497–4523.
Van de Wal, R.S.W., 1999. The importance of thermodynamics for modeling the volume of the Greenland ice sheet. Journal of Geophysical Research 104, 3887–3898.
Van den Berg, J., van de Wal, R.S.W., Oerlemans, J., 2006. Effects of spatial discretization in ice-sheet modelling using the shallow-ice approximation. Journal of Glaciology 52, 89–98.
Van Tatenhove, F.G.M., van der Meer, J.J.M., Huybrechts, P., 1995. Glacial–geological geomorphological research in west Greenland used to test an ice-sheet. Quaternary Research 44 (3), 317–327.
Van Tatenhove, F.G.M., van der Meer, J.J.M., Koster, E.A., 1996. Implications for deglaciation chronology from new AMS age determinations in central west Greenland. Quaternary Research 45 (3), 245–253.
Vieli, A., Funk, M., Blatter, H., 2001. Flow dynamics of tidewater glaciers: a numerical modelling approach. Journal of Glaciology 47 (159), 595–606.
Vieli, A., Payne, A.J., 2005. Assessing the ability of numerical ice sheet models to simulate grounding line migration. Journal of Geophysical Research – Earth Surface 110, F1.
Washburn, A.L., Stuiver, M., 1962. Radiocarbon-dated post-glacial deleveling in northeast Greenland and its implications. Arctic 15, 66–73.
Weidick, A., 1972. Holocene shore-lines and glacial stages in Greenland – an attempt at correlation. Rapport Grønlands Geologiske Undersøgelse 41, 1–39.
Weidick, A., 1976. Glaciation and the Quaternary of Greenland. In: Escher, A., Watt, W.S. (Eds.), Geology of Greenland. Geological Survey of Greenland, Copenhagen, pp. 405–458.
Weidick, A., Oerter, H., Reeh, N., Thomsen, H.H., Thorning, L.S., 1990. The recession of the Inland Ice margin during the Holocene climatic optimum in the Jakobshavn Isfjord area of West Greenland. Palaeogeography, Palaeoclimatology, Palaeoecology 82, 389–399.
Weidick, A., 1993. Neoglacial change of ice cover and the related response of the Earth's crust in west Greenland. Rapport Grønlands Geologiske Undersøgelse 159, 121–126.
Weidick, A., Bennike, O., 2007. Quaternary glaciation history and glaciology of Jakobshavn Isbrae and the Disko Bugt region, west Greenland: a review. Geological Survey of Denmark and Greenland Bulletin 14.
Weidick, A., Kelly, M., Bennike, O., 2004. Late Quaternary development of the southern sector of the Greenland ice sheet, with particular reference to the Qassimiut lobe. Boreas 33 (4), 284–299.
Wilken, M., Mienert, J., 2006. Submarine glacigenic debris flows, deep-sea channels and past ice-stream behaviour of the east Greenland continental margin. Quaternary Science Reviews 25 (7–8), 784–810.
Yokoyama, Y., Lambeck, K., De Dekker, P., Johnston, P., Fifield, L.K., 2000. Timing of the Last Glacial Maximum from observed sea-level minima. Nature 406 (6797), 713–716.
Zreda, M., England, J., Phillips, F., Elmore, D., Sharma, P., 1999. Unblocking of the Nares Strait by Greenland and Ellesmere ice-sheet retreat 10,000 years ago. Nature 398 (6723), 139–142.
Zweck, C., Huybrechts, P., 2003. Modeling the marine extent of northern Hemisphere ice sheets during the last glacial cycle. Annals of Glaciology 37, 173–180.
Zweck, C., Huybrechts, P., 2005. Northern hemisphere ice sheet modeling of the last glacial cycle and glaciological sensitivity. Journal of Geophysical Research 110, D07103.